Modelling glacier mass balance and runoff in the Kaskawulsh River headwaters of southwest Yukon, Canada, 1980–2022

Katherine M. Robinson[1], Gwenn E. Flowers[1], Michel Baraër[2], David R. Rounce[3]

[1]*Department of Earth Sciences, Simon Fraser University, Burnaby, BC, Canada*

[2]*Département de génie de la construction, École de Technologie Supérieure, Montréal, QC, Canada*

[3]*Civil and Environmental Engineering Department, Carnegie Mellon University, Pittsburgh, PA, USA*

Correspondence: Katherine Robinson <kmr18@sfu.ca>

This is a non-peer-reviewed preprint submitted to *EarthArXiv*. This manuscript has been submitted for publication in *Hydrological Processes*.

Modelling glacier mass balance and runoff in the Kaskawulsh River headwaters of southwest Yukon, Canada, 1980–2022

Katherine M. Robinson[1], Gwenn E. Flowers[1], Michel Baraër[2], David R. Rounce[3]

[1] *Department of Earth Sciences, Simon Fraser University, Burnaby, BC, Canada*

[2] *Département de génie de la construction, École de Technologie Supérieure, Montréal, QC, Canada*

[3] *Civil and Environmental Engineering Department, Carnegie Mellon University, Pittsburgh, PA, USA*

Correspondence: Katherine Robinson <kmr18@sfu.ca>

ABSTRACT. The highly-glacierized headwaters of the Kaskawulsh River are home to 9% of all glacier ice in Yukon, Canada, have been losing glacier mass at regionally representative rates, and were the source of a sudden meltwater-rerouting event in 2016 that has had significant downstream consequences. We use an enhanced temperature-index melt model driven by downscaled and bias-corrected climate reanalysis data to estimate the 1980–2022 glacier mass balance, discharge, and water budget of the Kaskawulsh River headwaters. We estimate a catchment-wide cumulative mass loss of 18.02 Gt over 1980–2022 ($-0.38 \pm 0.15\,\mathrm{m\,w.e.\,a^{-1}}$) and a mean annual discharge of $\sim 60\,\mathrm{m^3\,s^{-1}}$, 25% of which originates from non-renewable glacier wastage. The water budget is dominated by glacier ice melt, accounting for 61% of mean annual discharge, followed by snowmelt at 31%, rainfall at 6%, and melt from refrozen ice layers at 2%. Extreme negative and positive mass-balance years produce the largest perturbations in glacier ice melt contributions to the water budget, ranging from a maximum of 67% following negative years to a minimum of 53% in positive years. Catchment-wide discharge increased by $3.90\,\mathrm{m^3\,s^{-1}}$ per decade from 1980–2022, with statistically significant contributions from glacier ice melt ($2.80\,\mathrm{m^3\,s^{-1}}$ per decade) and rainfall ($0.47\,\mathrm{m^3\,s^{-1}}$ per decade). Rising air temperatures and declining spring snowfall have lead to seasonally accelerated

snowline retreat, earlier ice exposure, and earlier onset of net ablation in the catchment at a rate of ∼5 days per decade. Based on summer air temperatures projected by CMIP6, and the empirical sensitivities of modelled runoff we calculate for 1980–2022, we hypothesize a more than doubling of annual runoff from this catchment by 2080–2100. This result, combined with a decrease in the variability of discharge from glacier ice melt over 1980–2022, suggests that this catchment is unlikely to reach "peak water" (i.e. peak glacier contribution to catchment runoff) this century.

1 INTRODUCTION

Glacier-fed rivers play a critical role in many large-scale drainage basins around the world (e.g. Huss and Hock, 2018). In some basins, runoff contributions from glacier-ice melt are expected to increase by the end of the century, while other basins are projected to see reductions in runoff from glacier melt associated with declining glacier area (Huss and Hock, 2018). Global modelling efforts (e.g. Huss and Hock, 2018; Bliss and others, 2014) suggest that this turning point, referred to in the literature as "peak water", has already been reached in nearly half of global glacierized basins, while the remaining basins are likely to reach peak water before the end of the century. Glaciers in Yukon and Alaska are some of the largest contributors to present day global glacier mass loss (Zemp and others, 2019; Hugonnet and others, 2021), and are projected to continue to be among the most significant contributors in the future (Rounce and others, 2023). In Yukon, some small watersheds (2–9% glacierized) have likely already passed peak water (Chesnokova and others, 2020), while other large basins like the Alsek River and Yukon River basins, with $\sim 20\%$ glacier cover each, are expected to reach peak water between mid- to late century, depending on the emissions scenario (Huss and Hock, 2018).

Here, we employ a distributed mass-balance model (Young and others, 2021; Robinson and others, in review) to reconstruct four decades of mass balance, runoff, and water budget in a highly-glacierized, ungauged catchment in southwest Yukon. This catchment has, at different times in the recent past, contributed to runoff in both the Yukon River and Alsek River basins (Shugar and others, 2017). Ongoing mass loss throughout this region is producing changes in the timing and magnitude of freshwater that is delivered to the Gulf of Alaska (e.g. Neal and others, 2010), with potentially significant downstream impacts on the sediment and chemical fluxes to near-shore ecosystems (e.g. Hood and Berner, 2009) and future salmon habitat quality and range (e.g. Moore and others, 2023; Pitman and others, 2021). With a mean temperature increase of $7.8\,^{\circ}\mathrm{C}$ and a 24% increase in annual precipitation projected for northwestern North America by 2081–2100 relative to 1981–2010 under SSP5-8.5 (IPCC, 2021), it is important to understand how runoff contributions from highly-glacierized catchments in this region are changing. However, direct observations of glacier runoff via repeated measurements or continuous gauging (e.g. La Frenierre and Mark, 2014) are challenging, particularly in remote mountainous catchments, due to the inaccessibility of these sites and the difficulties associated with installing and maintaining gauges in dynamic proglacial streams (e.g. Goss, 2021). Modelling approaches that integrate available in-situ data offer an alternative method to reconstruct and partition the historical runoff record (e.g. Li and others, 2020; Azam and Srivastava, 2020), helping to overcome the limitations of field-based measurements by combining available observations with remote-sensing and climate reanalysis data.

The mass-balance model employed in this study is tailored to the catchment using in-situ data and tuned using site-specific remotely-sensed observations (Robinson and others, in review). It is then used to estimate the catchment-wide annual discharge contributions from ice melt, snowmelt, and rainfall. We analyze trends in the modelled mass balance and discharge and examine correlations between the modelled climate and discharge to identify the drivers of these trends. We also identify factors that produce extremes in the record and use these findings to generate hypotheses about possible future hydrological changes in this regionally significant catchment.

2 STUDY AREA

The hydrological catchment that encompasses the Kaskawulsh Glacier, hereafter referred to as the Kaskawulsh River headwaters (Figure 1), is a large (1704 km^2), 69% glacierized area located in the St. Elias Mountains of Yukon, Canada, within the Traditional Territories of the Kluane, Champagne & Aishihik, and White River First Nations. The Kaskawulsh Glacier itself is an $\sim$70 km long valley glacier spanning an elevation range of 750–3500 m a.s.l. (Fig. S1), and accounts for 93% of the glacierized area in the catchment and $\sim$9% of the glacier-ice volume in Yukon (Farinotti and others, 2019). The Kaskawulsh Glacier is situated on the continental side of the St. Elias Mountains and flows eastward from the ice divide with Hubbard Glacier (Clarke and Holdsworth, 2002), with four major tributaries contributing to the main trunk, which terminates at the drainage divide between the Yukon and Alsek River watersheds (Shugar and others, 2017). Approximately 14 other glaciers are located within the catchment, nearly all of which are $<$10 km^2 and unnamed.

Ongoing glacier mass loss and retreat in this region have already had pronounced effects on landscape evolution through retreat-driven river reorganization (e.g. Shugar and others, 2017), and through the formation and growth of new proglacial lakes (e.g. Main and others, 2023). The Kaskawulsh Glacier has been in a state of negative mass balance for several decades, with estimated mass loss rates of $0.46 \pm 0.20\,\mathrm{m\,w.e.\,a^{-1}}$ between 1977–2007 (Berthier and others, 2010) and $0.46 \pm 0.17\,\mathrm{m\,w.e.\,a^{-1}}$ between 2007–2018 (Young and others, 2021). An additional 23 km of committed terminus retreat is estimated under the 2007–2018 mean climate (Young and others, 2021), even without further warming. The glacier has been slow to adjust to its mass imbalance, with just 1.5% reduction in glacier area between 1977–2007 and 655 m of terminus retreat from 1956–2007 (Foy and others, 2011). Terminus retreat has also been associated with the formation and growth of two proglacial lakes (Shugar and others, 2017; Main and others, 2023). In May 2016, the abrupt drainage of one of these lakes caused meltwater that flowed north via the Ä'äy Chù (Slims River) to Łhù'ààn Mân (Kluane Lake), the Donjek River, White River, Yukon River, and ultimately discharging to the Bering Sea to be diverted south via the Kaskawulsh River (Figure 1), a tributary to the Alsek River that eventually discharges into the Gulf of Alaska (Shugar and others, 2017).

The rerouting event had many downstream consequences, including reduced water levels in Łhù'ààn Mân, and increased dust emissions from the Ä'äy Chù floodplain (e.g. Huck and others, 2023; Bachelder and others, 2020; Shugar and others, 2017). This event was also associated with an increase in braiding intensity and sediment erosion on the Kaskawulsh River, driven by the abrupt increase in discharge (Goss, 2021). Prior to the drainage reorganization, terminus velocities were increasing steadily over the period 2000–2012 at an average rate of $3\,\mathrm{m\,a^{-2}}$, but have since rapidly decelerated over 2015–2021 at a rate of $-12.5\,\mathrm{m\,a^{-2}}$ (Main and others, 2023). The slowdown and stagnation over parts of the terminus region are believed to be linked to a reduction in flotation caused by the proglacial lake drainage (Main and others, 2023).

3 METHODS

3.1 Mass-balance model

The distributed mass-balance model used in this study is adapted from Young and others (2021) (see S§1), with the addition of a surface-elevation parameterization, a glacier-specific representation of sub-debris ablation and an accumulation bias correction detailed in Robinson and others (in review) and Robinson (2024). The climatic mass balance $\dot{b}_{\mathrm{sfc}}(x, y)$ is calculated as the difference between surface accumulation $\dot{c}_{\mathrm{sfc}}(x, y)$ and surface ablation $\dot{a}_{\mathrm{sfc}}(x, y)$. Ablation is approximated as surface melt minus meltwater that is refrozen. Melt is calculated using the enhanced temperature-index model of Hock (1999), which improves upon the classical degree-day model by capturing the influence of topographic shading, slope, and aspect on melt through incorporating a radiation factor and calculated potential direct clear-sky solar radiation. The impact of supraglacial debris cover on ablation is treated using a distributed estimate of sub-debris melt factors, which either enhance or inhibit ice melt depending on the debris thickness. The sub-debris melt factors are based on an estimate of debris thickness for the Kaskawulsh Glacier from Rounce and

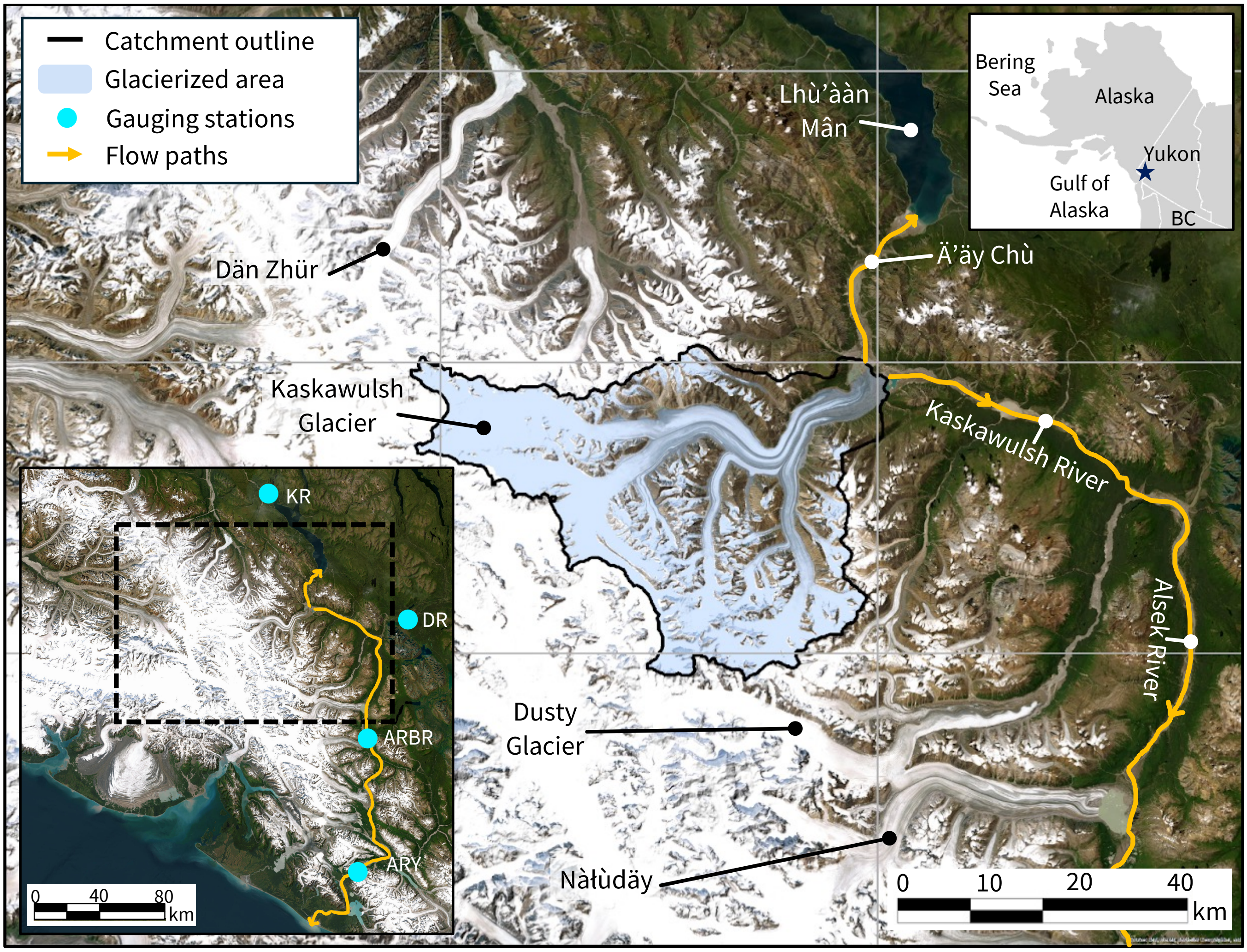

Fig. 1. Study area (blue star, inset) and overview of the surrounding glaciers (black text) and hydrological systems (white text). Blue shading indicates the glacierized area, with the boundary of the Kaskawulsh River headwaters outlined in black. Inset at bottom left shows the locations of four hydrometric gauging stations, operated by Environment and Climate Change Canada: Kluane River at the outlet of Kluane Lake (KR), Dezadeash River (DR), and Alsek River above Bates River (ARBR), and one station operated by the United States Geological Survey: Alsek River near Yakutat (ARY). Basemap sources: Esri, Maxar, Earthstar Geographics, and the GIS User Community.

others (2021) and a glacier-specific estimate of the Østrem curve (Robinson and others, in review), that is, a function that describes the relationship between debris thickness and ablation (Østrem, 1959). Meltwater retention via refreezing is accounted for using a thermodynic parameterization to estimate the annual potential retention mass (Janssens and Huybrechts, 2000). Once this limit is reached, any additional snowmelt or rainfall is assumed to run off (e.g. Huybrechts and De Wolde, 1999; Janssens and Huybrechts, 2000).

Catchment-wide discharge is the sum of all sources of runoff over the glacierized and non-glacierized areas (e.g. Bliss and others, 2014):

$$Q = M_{\text{glacier ice}} + M_{\text{snow}} + M_{\text{refrozen snowmelt/rain}} + P_l - R, \tag{1}$$

including glacier-ice melt ($M_{\text{glacier ice}}$), snowmelt (M_{snow}), ice melt from the refrozen snowmelt/rain layers formed during previous refreezing events ($M_{\text{refrozen snowmelt/rain}}$), and rainfall ($P_l$), minus the snowmelt and rainfall that are refrozen (R). Ice formed from refrozen snowmelt/rain is treated as superimposed ice in the ablation zone and internal accumulation in the accumulation zone. Snowmelt refers to melt of both the seasonal snowpack and snow accumulation that has persisted from previous seasons, as we do not account for the transition from snow to firn. Snowmelt, rainfall, and refreezing are treated the same over the non-glacierized area as the glacierized area of the catchment. We assume that all runoff instantaneously exits the catchment, that is, we do not account for transit times, supraglacial ponding, or englacial/subglacial storage, all of which would delay or reduce the estimated discharge (e.g. Huss and Hock, 2018). Our objective is to examine temporal trends in discharge, rather than to precisely reconstruct the daily discharge timeseries, thus neglecting a time-delay in modelled discharge does not affect the conclusions of the study. Furthermore, without in-situ discharge data to constrain the transit time, attempting to reconstruct the daily discharge timeseries would introduce further uncertainty and therefore be only speculative.

We also neglect runoff losses from sublimation, evapotranspiration, and infiltration. Some groundwater may be lost to the Ä'äy Chù, while some may resurface proglacially and discharge into the Kaskawulsh River, although these amounts are likely small: in the broader Alsek River Basin, estimated losses due to evapotranspiration and infiltration from non-glacierized areas are 5–40 $\mathrm{mm\,a^{-1}}$, accounting for 1–7% of the mean annual precipitation (Chesnokova and others, 2020). Sublimation losses are likely also small. On a small glacier on the northern side of the catchment, a point-scale estimate of sublimation was less than 1% of the total ablation estimated during the 2008 melt season (Wheler and Flowers, 2011).

The glacierized area is based on outlines from the Global Land Ice Measurements from Space inventory (GLIMS) Randolph Glacier Inventory (RGI 6.0) (RGI Consortium, 2017) (Kaskawulsh Glacier RGI ID: 60-01.16201) and is fixed throughout the simulation period (1980–2022). Surface elevation of the glacierized area is updated annually based on a smoothed estimate of the average annual elevation-change rate between 1977–2018 (Robinson and others, in review). The model is initialized with an entirely snow-free surface such that all glacierized areas are comprised of bare ice. We allow the glacier accumulation area to develop over the first year of the simulation, during which the snowpack builds up and is carried over year to year. This initial spin-up year is discarded from the analysis. The equilibrium line altitude (ELA) and accumulation area ratio (AAR) are transient outputs of the model rather than being prescribed.

3.2 Climate data

3.2.1 Temperature

The temperature and precipitation data used to drive the mass-balance model (Figure 2) are obtained by downscaling and bias correcting the North American Regional Reanalysis (NARR) dataset (Mesinger and others, 2006). NARR data are available beginning in 1979 and include gridded outputs for a suite of meteorological variables at 3-hourly timesteps on a $32\,\mathrm{km} \times 32\,\mathrm{km}$ grid. To obtain the temperature inputs for the melt model, the NARR temperature data are downscaled to a 200 m grid (Young and others, 2021) over the catchment using a linear interpolation scheme from Jarosch and others (2012) and bias-corrected following the approach of Young and others (2021).

3.2.2 Precipitation

The precipitation downscaling procedure follows a regression-based approach from Guan and others (2009), adopted by Young and others (2021), that relates NARR surface precipitation to the geographic predictors of precipitation (Easting, Northing and elevation) from 13 NARR gridcells on the continental side of the St. Elias Mountains and orographic divide (Robinson, 2024). Accumulation is estimated from 200 m downscaled NARR precipitation partitioned into rain and snow using a prescribed temperature threshold of 1°C (Young and others, 2021). Downscaled accumulation is bias corrected with an elevation-dependent function developed by Robinson and others (in review) using 27 in-situ measurements of snow depth and density at 18 different locations within the catchment made between 2007–2022. Within the Kaskawulsh River headwaters, NARR generally underestimates measured seasonal accumulation, with biases generally

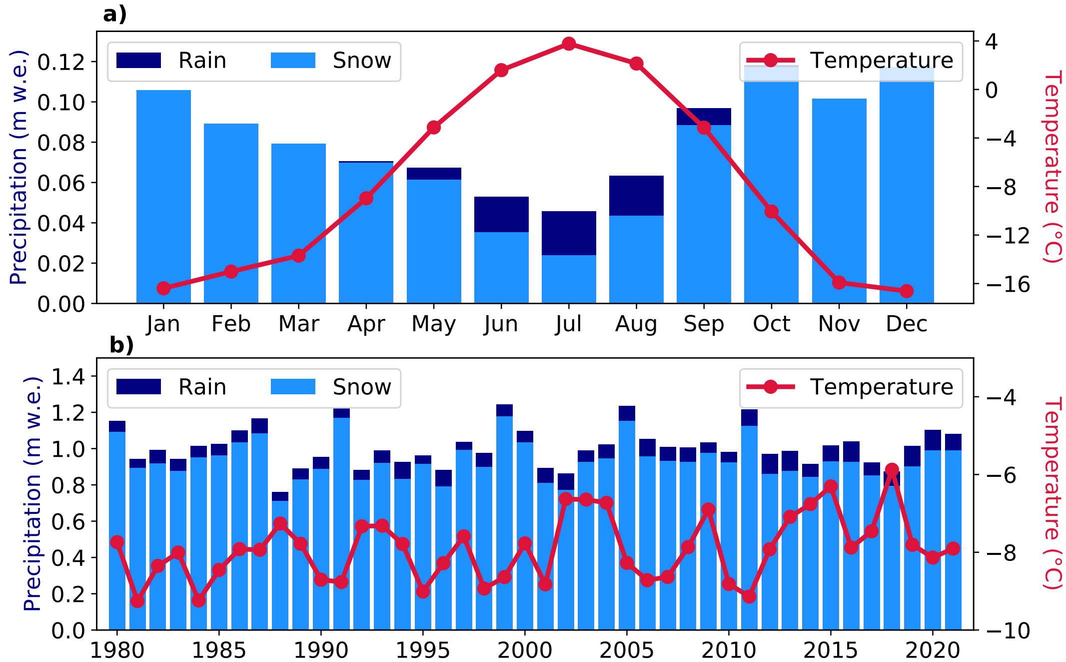

Fig. 2. Downscaled and bias corrected North American Regional reanalysis data averaged over the Kaskawulsh River headwaters. (a) Monthly average temperature (red line) and precipitation partitioned into snow and rainfall using a temperature threshold of 1°C (light blue: snow, dark blue: rainfall). (b) Mean annual temperature and total precipitation from 1980–2022. Note that units for precipitation are meters water equivalent (m w.e.), representing the volume of water divided by the catchment area.

increasing with elevation. Bias-corrected accumulation shows improved agreement with airborne-radar-derived accumulation estimates from NASA's Operation IceBridge (OIB) in May 2021 (Li and others, 2023), with a 67% reduction in the mean absolute error between measured and modelled accumulation relative to downscaled, uncorrected accumulation data (Robinson and others, in review). In the absence of reliable in-situ rainfall data, the liquid component of downscaled precipitation is not bias corrected.

3.3 Model tuning

The melt- and radiation factors for snow and ice used in the enhanced-temperature index model (Hock, 1999) are determined through a tuning process from Robinson and others (in review) based on two empirical tuning targets: (a) the 2007–2018 glacier-wide geodetic mass balance (Young and others, 2021) and (b) observed snow cover determined by transient snowline positions delineated from over 50 satellite images between 2013–2019. We impose the constraint that the radiation factor for ice must be larger than that for snow (e.g. Hock, 1999, 2003; Young and others, 2018), since snow generally has a higher albedo than bare ice (e.g. Warren, 2019). Initially, 10,000 simulations are performed using combinations of the three melt-model parameters randomly sampled from independent normal distributions defined by the mean and standard deviations of these values found in the literature (e.g. Young and others, 2021). The final simulations are selected such that the ensemble forms a normal distribution defined by the mean and standard deviation of the geodetic mass balance, encompassing exactly 100 simulations. The results and uncertainties presented in this paper are based on the mean and standard deviations of the 100-simulation ensemble. This procedure guarantees that the mean modelled 2007–2018 mass balance is identical to the empirical target ($-0.46 \pm 0.17\,\mathrm{m\,w.e.\,a^{-1}}$), while retaining simulations that best reproduce the transient snowline position.

3.4 Hydrological data

Discharge from the Kaskawulsh River headwaters catchment historically flowed into two drainage basins: the Yukon River basin to the north via Ä'äy Chù and the Alsek River basin to the south via Kaskawulsh River (Figure 1). In May 2016, the retreat of Kaskawulsh Glacier triggered a drainage reorganization in which melt water from the Ä'äy Chù was captured by the Kaskawulsh River, which has a lower base level than the Ä'äy Chù, ultimately increasing the supply of water to the Alsek River (Shugar and others, 2017). We estimate the contribution of the Kaskawulsh River headwaters catchment to discharge on the Alsek River since the 2016 drainage reorganization using discharge data from two downstream hydrometric stations. Neither the Kaskawulsh River nor the Ä'äy Chù is gauged near the glacier terminus, precluding direct comparisons between modelled and measured discharge from the catchment.

Environment and Climate Change Canada (ECCC) maintains a hydrometric station on the Alsek River above Bates River (60.118 °N,−137.978 °W), located just above Fisher Glacier, roughly 110 km downstream from the Kaskawulsh Glacier terminus (Figure 1). The gross drainage area at this location is 16,200 $\mathrm{km^2}$, and includes other large glaciers south of the Kaskawulsh Glacier, such as Dusty Glacier and Nàłùdäy (Lowell Glacier). Daily discharge measurements at this station are available from 1974–2019. The ECCC Historical Hydrometric Data web site (https:wateroffice.ec.gc.camainmenuhistorical_data_index_e.html) notes that particularly high flows were recorded in 2016 after meltwater from the Kaskawulsh Glacier was rerouted to the Alsek River. The drainage area also includes the Dezadeash River catchment (8450 $\mathrm{km^2}$), a tributary catchment to the Alsek River where discharge is artificially controlled for hydroelectricity production. Another hydrometric station operated by the United States Geological Survey (USGS) is located 120 km further downstream from the Bates River junction with the Alsek River at 59.395 °N, −138.082 °W (Figure 1). This station is near Yakutat, Alaska, about 60 km upstream of where the Alsek River discharges to the North Pacific Ocean, and has a gross drainage area of 28,500 km^2.

3.5 Trend detection

Hydrological changes over the four-decade study period are identified by examing the absolute and relative contributions to total discharge from each modelled source: glacier-ice melt, snowmelt, rainfall, and melt of ice formed from refrozen snowmelt/rain over time. We apply the Mann-Kendall and Modified Mann-Kendall statistical tests to the modelled discharge timeseries over 1980–2022 to identify the significance and magnitude of these changes.

The Mann-Kendall test is a non-parametric test used to identify monotonic positive or negative trends in a timeseries (Kendall, 1948; Mann, 1945). The test, based on the relative differences between pairs of observations (ranks), reduces the influence of outliers in the data but relies on the assumption that the observations are independent of one another. Positive serial correlation between successive values can therefore bias this test, and is accounted for in the Modified Mann-Kendall test by adjusting the sample size of the data to reflect the fact that not all values in the timeseries are independent of one another (Hamed and Rao, 1998). As a result, the Modified Mann-Kendall test has a decreased rate of falsely identifying trends in autocorrelated data compared to the original Mann-Kendall test. We reject the null hypothesis, which assumes no monotonic trend in the timeseries, based on the arbitrary but common significance level of α=0.05. The magnitude of statistically significant trends is estimated using Sen's slope, which is commonly used in conjuction with the Mann-Kendall test, and is the median slope between all possible pairs of data points in the timeseries, resulting in an estimate that reduces the influence of outliers (Sen, 1968).

Following Chesnokova and others (2020), we apply the Mann-Kendall and Modified Mann-Kendall statistical tests to a suite of variables that characterize the hydrological regime of the catchment (Table 1), and consider the results of both tests to identify persistent trends in discharge over time. We evaluate the mean discharge over key seasonal periods and the timing of the onset of the ablation season and peak discharge to detect shifts in the seasonal discharge pattern. We also assess trends in discharge variability across different time frames to evaluate whether the catchment has passed the peak water threshold. Decreased variability in conjunction with increased ablation-season discharge may suggest that a catchment

Variable	Description	Units
Q_{annual}	Mean discharge over the hydrological year (Oct–Sept)	$\mathrm{m^3\,s^{-1}}$
Q_{abl1}	Mean July–August discharge	$\mathrm{m^3\,s^{-1}}$
Q_{abl2}	Mean May–August discharge	$\mathrm{m^3\,s^{-1}}$
Q_{w}	Mean winter discharge (November–March)	$\mathrm{m^3\,s^{-1}}$
Q_{max5d}	Mean 5-day maximum discharge	$\mathrm{m^3\,s^{-1}}$
D_{max5d}	Day of year corresponding to Q_{max5d}	day of year
D_{abl}	The first day of the year with a daily discharge $> 0\,\mathrm{m^3\,s^{-1}}$	day of year
CV_{annual}	Coefficient of variation for Q_{annual}	unitless
CV_{abl1}	Coefficient of variation for Q_{abl1}	unitless
CV_{abl2}	Coefficient of variation for Q_{abl2}	unitless

Table 1. Variables used to identify hydrological changes over time, computed from the modelled daily discharge timeseries.

is headed towards peak water, with increasing influence from the glacierized area, while increased variability with decreased discharge may indicate that peak water has passed, leading to less predictable runoff as glacier ice melt declines (e.g. Baraër and others, 2012; Chesnokova and others, 2020).

3.6 Estimating future changes in discharge

We examine the relationships between modelled discharge and changes in the mass balance and climate over the study period to identify possible drivers of changes to the hydrological regime. To assess the strength of any relationship between two variables, we apply Spearman's correlation test, another non-parameteric test based on the correlation between ranks of pairs of observations (Spearman, 1904). Relationships that exhibit statistically significant correlations are used to compute the sensitivity of modelled discharge to changes in the mass balance and/or climate over the study period. We estimate trend magnitudes between significantly correlated variables using a linear regression, and use these historical sensitivities to generate hypotheses about possible futures for the hydrological regime and water budget of the catchment.

To estimate future changes in climate in the study area, we use the results of the Coupled Model Intercomparison Project Phase 6 (CMIP6) for SSP5-8.5, a high-emissions scenario that represents the highest warming by 2100 of all CMIP6 scenarios (Gidden and others, 2019), and allows us to explore the maximum impact of climate change on discharge in the catchment within the bounds of CMIP6. We extract projected changes for the Kaskawulsh River headwaters from the $1^\circ \times 1^\circ$ CMIP6 gridcell with the greatest overlap with the catchment for three future time periods: near-term (2021–2040), medium-term (2041–2060), and long-term (2081–2100) relative to the historical period 1981–2010 (Gutiérrez and others, 2021). We then multiply the historical sensitivity to various climate variables by the projected change in any given variable for the three future time periods. The resulting change in discharge is added to the average discharge from 1981–2010 (estimated with the mass-balance model) to generate hypotheses about the future hydrological regime of the catchment.

4 RESULTS

4.1 Kaskawulsh River headwaters mass balance, discharge, and water budget from 1980–2022

Using the tuned mass-balance model, we reconstruct the 1980–2022 mass balance and discharge record from the Kaskawulsh River headwaters. We estimate that the cumulative mass loss from all ice in this catchment between 1980–2022 amounted to 18.02 Gt (Fig. 3a), with an average mass balance of $-0.40 \pm 0.16\,\mathrm{m\,w.e.\,a^{-1}}$ from the Kaskawulsh Glacier alone and $-0.38 \pm 0.15\,\mathrm{m\,w.e.\,a^{-1}}$ from all ice in the catchment. For several of the smaller glaciers on the periphery of the catchment, the model incorrectly predicts positive mass balances over the study period (e.g. Larsen and others, 2015), an artifact caused by the fact that none of the tuning data pertain to these small glaciers. However, these glaciers represent just 6.3% of ice in the catchment by area and cannot compensate for the negative balance estimated for the Kaskawulsh Glacier.

In each decade since the 1980s, the mean annual mass balance of the Kaskawulsh Glacier has become more negative (Table 2), indicating that mass loss may be accelerating. The seasonal onset of net ablation in the catchment, defined by the date where the annual (1 Oct–30 Sept) cumulative balance becomes negative, occurs by 28 July on average, however our modelling results suggest that the timing of this transition is occurring earlier in the melt season by approximately five days per decade (Fig. S2), and occurred as early as 28 June during strongly negative balance years.

Several years during the study period had net positive mass balances (Figure 3b), especially during the period 1980–1987 when the net balance of the catchment was frequently near zero with an average mass balance of $-0.04\,\mathrm{m\,w.e.\,a^{-1}}$. This period is associated with below-average annual temperatures and above-average snowfall, potentially linked to the Pacific Decadal Oscillation (PDO) (e.g. Brabets and Walvoord, 2009); there was a strong positive modal shift in the PDO index in 1976 which became briefly negative again

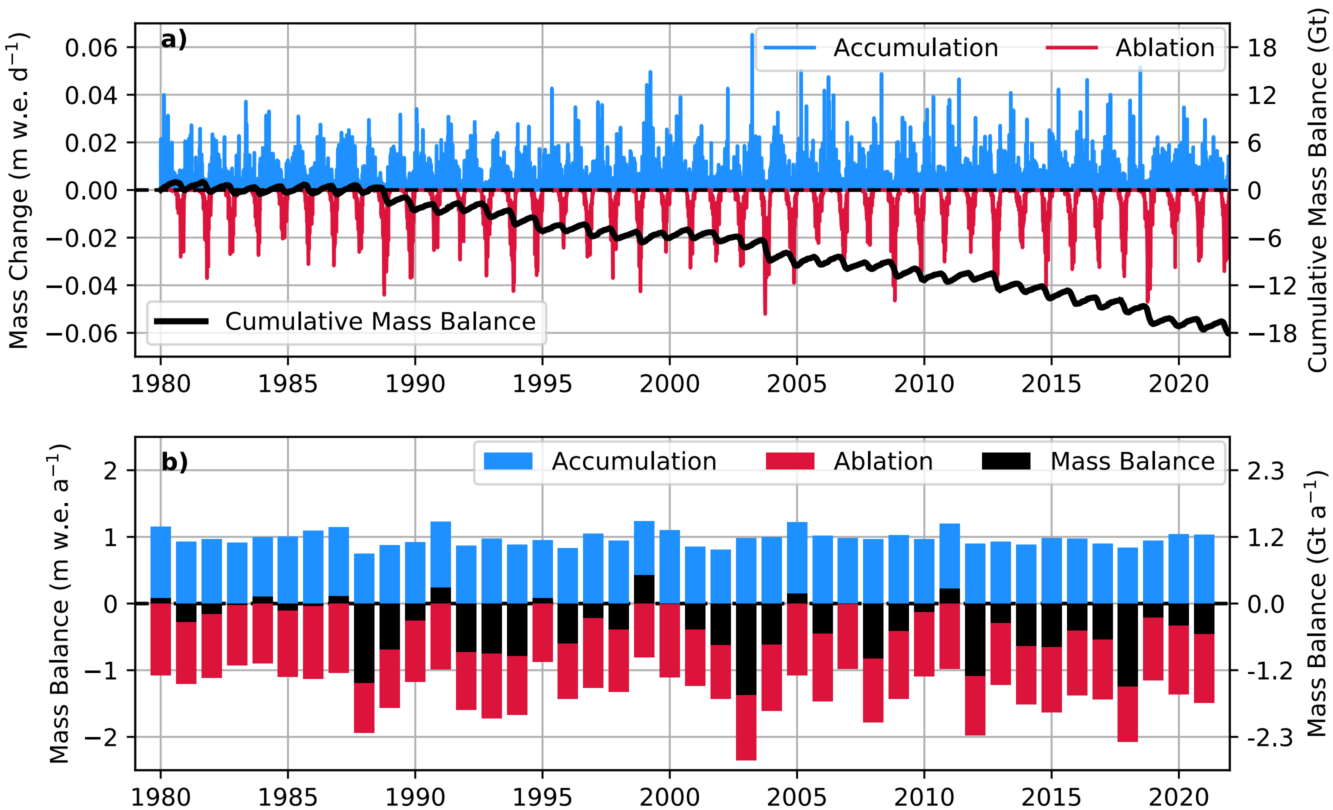

Fig. 3. Timeseries of daily and annual mass-balance components from 1980–2022. (a) Daily mean accumulation (blue) and ablation (red) over the glacierized area in the Kaskawulsh River headwaters catchment, and the cumulative mass balance (black) from 1980–2022 (−18.02 Gt). (b) Annual glacierized area-wide mean accumulation, ablation, and mass balance.

	Kaskawulsh Glacier mass balance (m w.e. a^{-1})	Catchment-wide mass balance (m w.e. a^{-1})	Total mass change (Gt)
1980-1989	-0.25 ± 0.14	-0.22 ± 0.13	-2.54 ± 1.55
1990-1999	-0.32 ± 0.15	-0.30 ± 0.14	-3.48 ± 1.69
2000-2009	-0.48 ± 0.17	-0.45 ± 0.16	-5.30 ± 1.93
2010-2019	-0.53 ± 0.18	-0.49 ± 0.17	-5.80 ± 1.97
2020-2022	-0.42 ± 0.16	-0.39 ± 0.16	-0.91 ± 0.37
1980-2022	$\mathbf{-0.40 \pm 0.16}$	$\mathbf{-0.38 \pm 0.15}$	$\mathbf{-18.02 \pm 7.51}$

Table 2. Mean mass balances from the Kaskawulsh Glacier alone and catchment-wide glacierized area (including Kaskawulsh Glacier). Uncertainties reported are the standard deviations of the 100 simulations that comprise the tuned mass-balance model.

around August 1988 (Mantua and Hare, 2002). However, the relationship between winter accumulation and the PDO remains largely ambiguous. While Foy and others (2011) found an increase in winter balances for certain glaciers in the Mount Logan region and southeast Alaska after the 1976 PDO shift, Moore and Demuth (2001) found a decrease in winter balances at Place Glacier in southern British Columbia. The Kaskawulsh River headwaters last experienced a positive net mass balance during the 2011–2012 balance year, making the past decade (2012–2022) the longest period of consecutive negative balance years in the study period by a factor of two (Figure 3b).

Modelled discharge is partitioned into four sources: glacier-ice melt, net snowmelt (total snowmelt minus refreezing), net rainfall (total rainfall minus refreezing), and melt from the refrozen snowmelt/rain layer. Early in the ablation season (late-April until approximately mid-June), the water budget is primarily influenced by snowmelt (Fig. 4b). Over the course of the ablation season however, glacier-ice melt becomes the predominant source of discharge, accounting for an average of 61% of the annual discharge, while snowmelt accounts for 31%, rainfall 6%, and melt of refrozen snowmelt/rain 2% (Figure 4b). Mean annual discharge from non-renewable glacier wastage (melt in excess of annual accumulation) is $14.9\,\mathrm{m^3\,s^{-1}}$, accounting for ~25% of the total mean annual discharge ($59.9\,\mathrm{m^3\,s^{-1}}$) on average between 1980–2022. However, in the three most negative mass-balance years, discharge from non-renewable glacier wastage makes up >50% of the annual discharge.

The annual peak in daily discharge is $530\,\mathrm{m^3\,s^{-1}}$ averaged over 1980–2022, with high interannual variability ranging from a minimum of $\sim350\,\mathrm{m^3\,s^{-1}}$ during some of the coldest hydrological years in the record

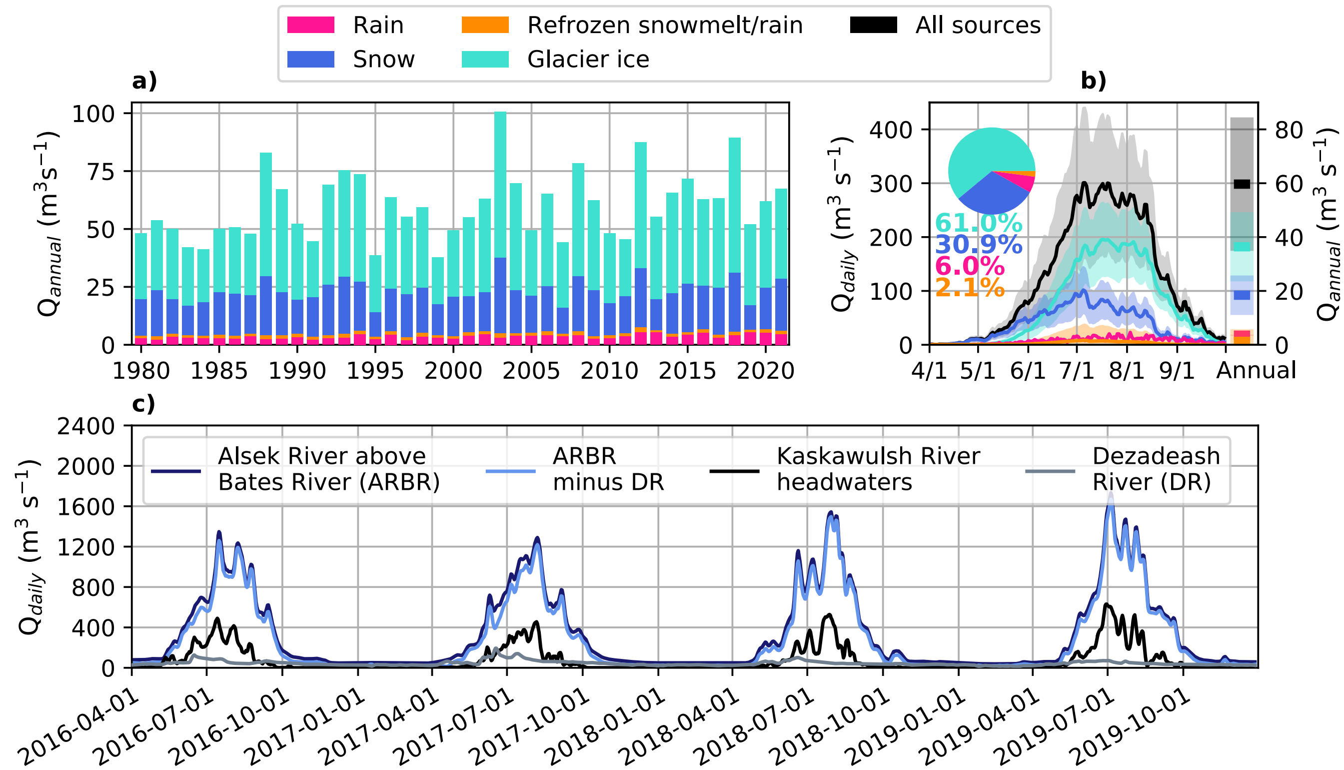

Fig. 4. Catchment-wide annual discharge and mean daily discharge from the four modelled sources from 1980–2022. (a) Annual discharge and (b) mean daily discharge from 1980–2022. Pie chart and percentages represent the fractional contributions from each source to total catchment-wide discharge, while bars on the right y-axis show the mean annual discharge from each source. Shading shows the standard deviation of the 100-simulation ensemble that comprise the tuned mass-balance model. (c) Daily modelled discharge from the Kaskawulsh River headwaters (this study, black line) and discharge measured at two downstream hydrometric stations.

(e.g. 1984–1985) and a maximum of $\sim$800 $\mathrm{m^3\,s^{-1}}$ during one of the warmest hydrological years in the record (2003–2004). The 2003–2004 hydrological year also saw the highest annual discharge during the study period (101 $\mathrm{m^3\,s^{-1}}$) (Figure 4a) and the most negative mass balance (-1.41 m w.e. $\mathrm{a^{-1}}$). The impact of these conditions and of other highly negative or positive mass-balance years on the composition of the water budget is discussed further in §4.4.1.

4.2 Contributions to the Alsek River

Mean annual discharge recorded at the hydrometric station on the Alsek River above Bates River (Figure 1) during the decade preceding the rerouting of melt water from Kaskawulsh Glacier (2005–2015) was 248.60 $\mathrm{m^3\,s^{-1}}$. This increased to 321.54 $\mathrm{m^3\,s^{-1}}$ (+72.94 $\mathrm{m^3\,s^{-1}}$) in 2016–2019 after melt water that previously entered the Ä'äy Chù was diverted south to the Kaskawulsh River, which flows into the Alsek River (Fig. S3). Using the tuned model, we estimate the mean annual discharge from the Kaskawulsh River headwaters from 2016–2019 to be $71.98 \pm 25.37\,\mathrm{m^3\,s^{-1}}$, consistent with the observed increase in discharge in the Alsek River after the drainage reorganization. This supports the idea that the observed increase in discharge on the Alsek River was driven by the hydrological reorganization, rather than natural variability in the downstream climatic conditions. Modelled discharge in the Kaskawulsh River headwaters over the 2015–2016 hydrological year was $71.66\,\mathrm{m^3\,s^{-1}}$, considerably higher than the historic (1980–2015) modelled annual discharge of $58.34\,\mathrm{m^3\,s^{-1}}$ (Figure 4a). Indeed Shugar and others (2017) hypothesized that warmer than average air temperatures and enhanced surface melt during the 2016 melt season led to the development and enlargement of an ice-walled channel connecting the two proglacial lakes, causing one of the proglacial lakes that previously drained into the Ä'äy Chù to drain into to the lower base-level Kaskawulsh River (Figure 1).

The Kaskawulsh River headwaters ($1704\,\mathrm{km^2}$) represent just over 10% of the total drainage area of the Alsek River above Bates River station ($16{,}200\,\mathrm{km^2}$), or 22% of the drainage area of the Alsek River above Bates River station if the Dezadeash River drainage ($8450\,\mathrm{km^2}$), a tributary to the Alsek River where discharge is artificially controlled for hydroelectricity production, is excluded. Modelled annual discharge from the Kaskawulsh River headwaters accounts for 19–26% of the annual discharge measured at the Alsek River above Bates River hydrometric station between 2016–2019, and modelled contributions from the Kaskawulsh River headwaters are largest in July when glacier-ice melt typically reaches a peak, amounting to 32% of the July discharge measured at the Alsek River above Bates River station (Fig. S4). Subtracting the annual discharge contributions from the Dezadeash River station (Figure 1), the estimated annual discharge from the Kaskawulsh River headwaters accounts for 22–29% of the annual discharge measured at the Alsek River above Bates River station (Figure 4c). While modelled discharge cannot be verified without direct measurements at the Kaskawulsh River headwaters, considering the substantial size of Kaskawulsh Glacier ($1099\,\mathrm{km^2}$) relative to the other major glaciers upstream of the ECCC hydrometric station, namely Dusty Glacier ($343\,\mathrm{km^2}$) and Nàłùdäy (Lowell Glacier) ($582\,\mathrm{km^2}$) (Arendt and others, 2017) and the fact that the relative contribution from the Kaskawulsh River headwaters is proportional to the fraction of the drainage area it represents, these estimations of discharge appear reasonable. The Kaskawulsh River headwaters also have a high specific discharge ($0.042\,\mathrm{m^3\,s^{-1}\,m^{-2}}$) relative to the drainage area of the Alsek River above Bates River station ($0.020\,\mathrm{m^3\,s^{-1}\,m^{-2}}$), likely due to the high fraction of glacierized area in the catchment.

Relative to the period 1980–1989, catchment-wide annual discharge increased by 6.5%, 18.9%, and 19.5% in each subsequent decade during the study period (Table S1). This increasing trend in modelled discharge is consistent with the trend in observed discharge downstream at the Alsek River above Bates River station, suggesting that the climatic changes driving increased discharge in the catchment affected discharge downstream as well (Fig S5). Relative to the mean annual discharge from 1980–1989 at the Alsek River above Bates River station ($219.11\,\mathrm{m^3\,s^{-1}}$), annual discharge at the station increased by 2.8% ($225.14\,\mathrm{m^3\,s^{-1}}$), 13.0% ($247.65\,\mathrm{m^3\,s^{-1}}$), and 27.5% ($279.36\,\mathrm{m^3\,s^{-1}}$) in each subsequent decade. If we subtract the modelled contributions from the Kaskawulsh River headwaters after 2016, discharge at the Alsek River above Bates River station still increased by 14.5% (cf. 27.5%) during 2010–2019 relative to 1980–1989.

Further downstream at the USGS hydrometric station on the Alsek River near Yakutat (Figure 1), annual discharge recorded during the period that the station was active (1993–2012) was $888.51\,\mathrm{m^3\,s^{-1}}$. Based on these values, an additional $71.98 \pm 25.37\,\mathrm{m^3\,s^{-1}}$ as modelled from the Kaskawulsh River headwaters catchment beginning in 2016 would have resulted in a 5–11% increase in annual discharge to the North Pacific Ocean.

4.3 Changes in hydrological regime

4.3.1 Shifts in glacier ice melt indicate pre-peak water phase

Catchment-wide annual discharge ($\mathrm{Q_{annual}}$) increased by $3.9\,\mathrm{m^3\,s^{-1}}$ per decade from 1980–2022 ($p = 0.006$), while mean May–August discharge (Q_{abl2}) increased by $10.2\,\mathrm{m^3\,s^{-1}}$ per decade ($p = 0.007$) (Figure 5). A large fraction of this increase in annual discharge is due to enhanced glacier-ice melt: both the Mann-Kendall and Modified Mann-Kendall tests found positive trends in mean annual discharge ($\mathrm{Q_{annual}}$), mean July–August discharge (Q_{abl1}), and mean May–August discharge (Q_{abl2}) from glacier-ice melt, the latter of which exhibits a statistically significant increase of $7.7\,\mathrm{m^3\,s^{-1}}$ per decade ($p = 0.0003$) based on the the Modified Mann-Kendall test (Figure 5). In addition, the mean 5-day maximum discharge ($\mathrm{Q_{max5d}}$), a measure of peak annual discharge, from glacier-ice melt exhibits statistically significant increases of $9.8\,\mathrm{m^3\,s^{-1}}$ per decade. Interannual discharge variability from glacier-ice melt ($\mathrm{CV_{annual}}$) decreased at a statistically significant rate (Figure 5), characteristic of a catchment in the early stages of deglaciation (Baraër and others, 2012). These patterns suggest that glacier-ice melt is exerting an increasing influence on catchment-wide discharge over time, as evidenced by both the increase in discharge and decrease in

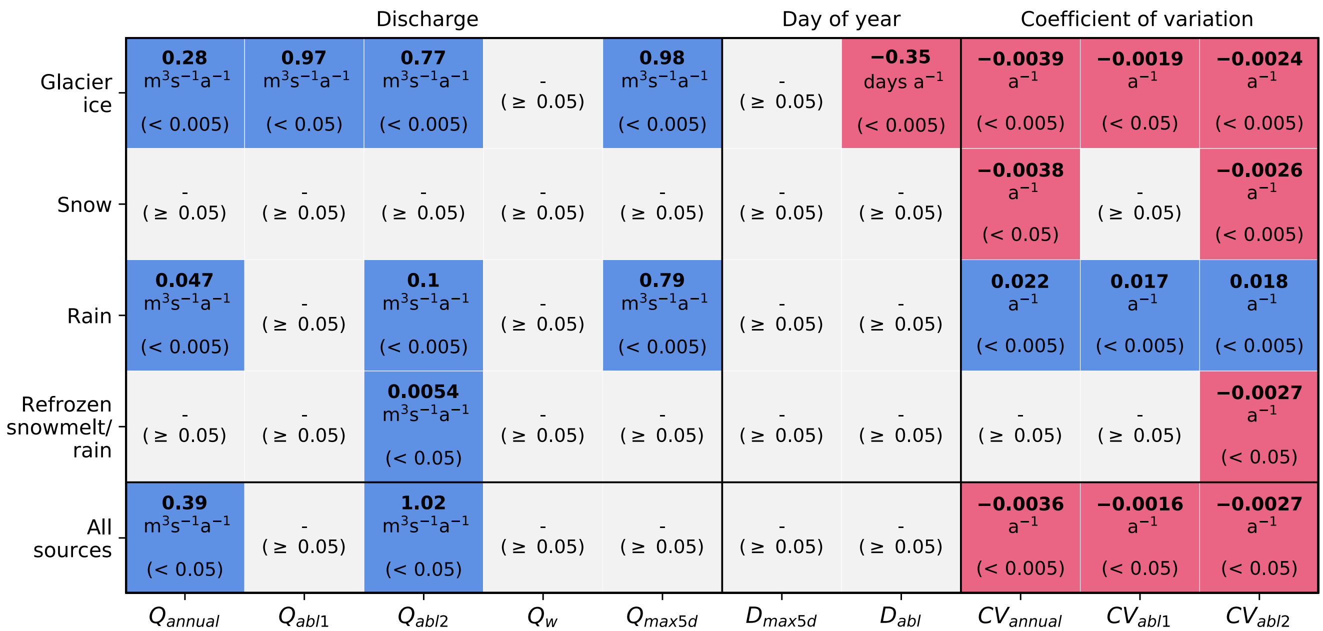

Fig. 5. Results of the modified Mann-Kendall test applied to the computed discharge variables (Table 1): Q_{annual} (mean annual discharge), Q_{abl1} (mean July–August discharge), Q_{abl2} (mean May–August discharge), Q_{w} (mean November–March discharge), Q_{max5d} (mean 5-day maximum discharge), D_{max5d} (day of year corresponding to Q_{max5d}), D_{abl} (first day of year with daily discharge > 0), CV_{annual} (coefficient of variation for Q_{annual}), CV_{abl1} (coefficient of variation for Q_{abl1}), and CV_{abl2} (coefficient of variation for Q_{abl2}). Blue squares indicate a statistically-significant positive trend, while red squares indicate a statistically-significant negative trend. Grey squares indicate no statistically-significant trend. Values reported inside each square are the magnitude of the trend (for statistically-significant trends only), with p-values in parentheses. See Fig. S6 for the original Mann-Kendall test results.

interannual discharge variability.

These trends may be explained in part by the increase in mean annual air temperatures over 1980–2022 (+0.021 °C a^{-1}, p=0.02). Decreased April snowfall (−0.65 mm w.e.,month^{-1}, p=0.03) (Figure 6b) may also leads to accelerated snowline retreat and earlier ice exposure in the melt season (Figure 6d), while increased snowfall in August and September (Figure 6b) can inhibit melt due to the albedo feedback (e.g. Naegeli and Huss, 2017). Although albedo is not explicitly included in our model, the tuning constraint requiring the radiation factor for ice to be larger than that for snow accounts for this feedback (e.g. Hock, 1999, 2003; Young and others, 2018). The model results suggest that early spring glacier-ice melt is increasing at a greater pace than late summer glacier-ice melt, producing an asymmetric shift in the seasonal discharge regime from glacier-ice melt (Figure 6e). While we find no significant trend in the timing of peak discharge ($\mathrm{D}_{\mathrm{max5d}}$), the date when discharge from glacier-ice melt begins ($\mathrm{D}_{\mathrm{abl}}$) exhibits a statistically significant shift, occurring earlier in the melt season by about 3.5 days per decade (Figure 5), consistent with the aforementioned increase in early summer ice melt (Figure 6e).

4.3.2 Trends in discharge from snowmelt and rainfall

Monthly discharge from snowmelt (Figure 6f) fluctuates following the observed trends in temperature (Figure 6a), rather than exhibiting monotonic trends like those observed in glacier-ice melt (Figure 6e,f). This suggests that discharge from snowmelt is closely related to the available melt energy. In accordance with the observed trend in positive degree-days in May (Figure 6a), snowmelt in May increased monotonically over each decade of the study period. However, there are no statistically significant trends in mean discharge from snowmelt over July–August (Q_{abl1}) or May–August (Q_{abl2}) (Table 1, Figure 5).

While snowmelt accounts for 20–39% of the annual water budget between 1980–2022 (Figure 4a), its relative importance may decrease over time due to the increased contributions from glacier-ice melt. Though annual snowfall may have decreased slightly over the study period (−0.001 m w.e. a^{-1}), the trend is not statistically significant. The fraction of annual precipitation occurring as rain, however, has increased at a statistically significant rate of ∼1% per decade (+0.001 m w.e. a^{-1}) between 1980–2022 (Fig. S8). While rainfall makes up just 2–11% of the annual catchment-wide water budget, annual discharge from rainfall increased 55% from 2.85 $m^3\,s^{-1}$ in 1980–1989 to 4.44 $m^3\,s^{-1}$ in 2010–2019, with particularly substantial increases in August and September (Figure 6g) in part due to increased air temperatures impacting the partitioning of precipitation into rain and snow during late summer/early fall. These changes point to

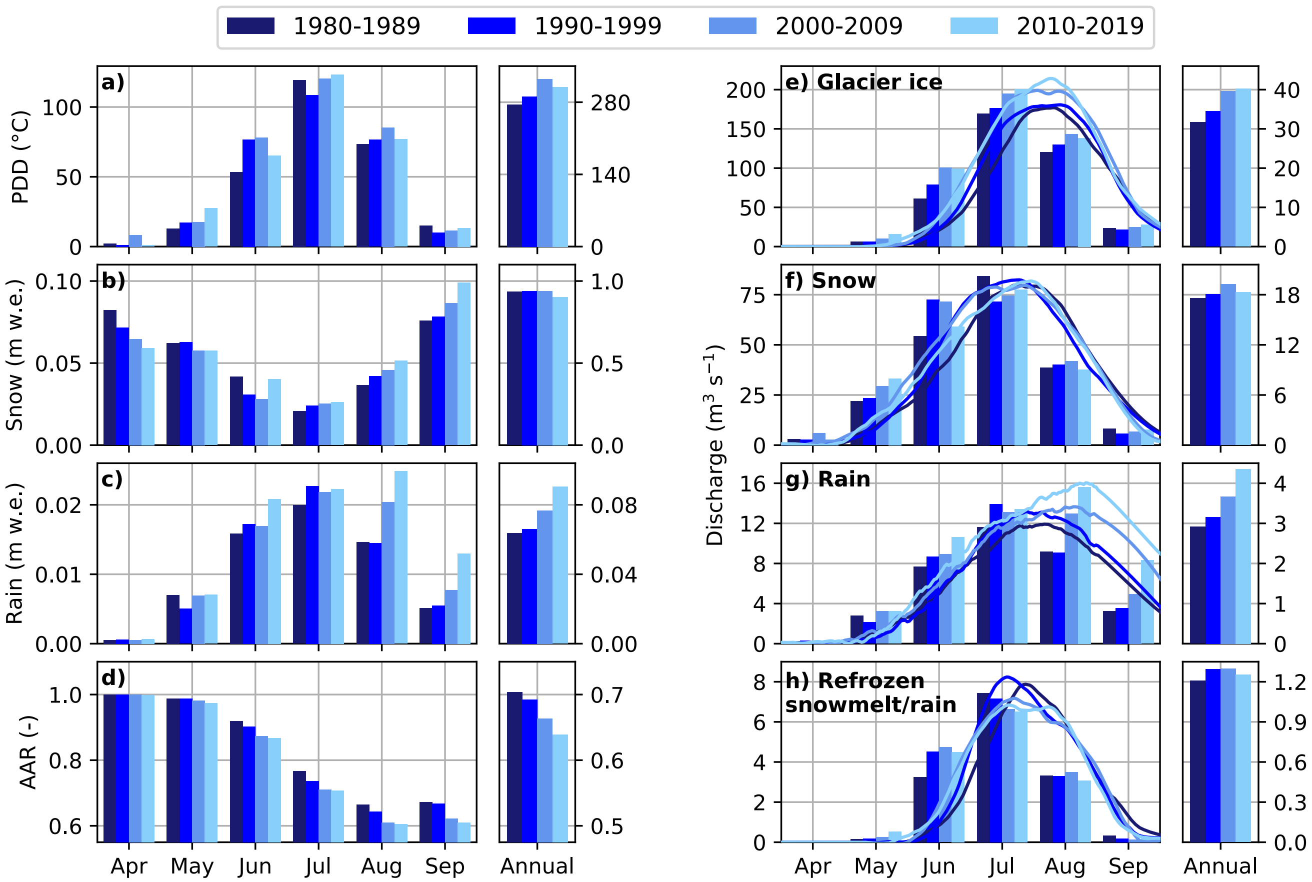

Fig. 6. Trends in climate, mass-balance, and discharge variables during the study period. (a–d) Monthly and annual (a) positive degree-day sum (PDD), (b) snowfall, (c) rainfall computed from downscaled and bias-corrected NARR precipitation partitioned into rain and snow using a temperature threshold of 1°C, and (d) transient accumulation area ratio (AAR). See Fig. S7/S8 for annual timeseries. July 1988 was anomalously warm, without which the 1980–1989 average PDD in (a) would be lower than the 1990–1999 average. Units for precipitation in (b,c) are meters water equivalent (m w.e.), representing the volume of water divided by the catchment area (i.e., the thickness of water distributed over the catchment area). (e–h) Catchment-wide monthly and annual discharge (bars), with decadally averaged daily discharge (lines) smoothed using a zero-phase-shift filter and a window size of 51 days (91 days for rainfall) (Fig S9). Note the difference in scales on the y-axes in (e–h).

rainfall becoming a more important contributor to discharge in the future. In contrast to glacier ice melt, rainfall saw an increase in discharge variability between 1980–2022, a trend consistent with an increase in rainfall intensity over the study period.

4.4 Drivers of extremes in the water budget and discharge record

4.4.1 Impact of mass balance on the water budget

Extreme negative mass-balance years (defined as annual mass balances in the bottom 5% of the study period) range from -1.23 to $-1.41\,\mathrm{m\,w.e.\,a^{-1}}$, while extreme positive mass-balance years (defined as the top 5%) range from 0.20 to $0.41\,\mathrm{m\,w.e.\,a^{-1}}$. Extreme negative years influence the catchment-wide water budget in the subsequent year through preconditioning the glacier surface for enhanced firn (treated as snow in the model) or ice melt. During a year with an extreme negative mass balance there is reduction in the accumulation area, yielding an increase in the relative contribution of glacier-ice melt to the water budget during the subsequent year (e.g. Figure 7). This preconditioning effect occurs even when the subsequent year's mass balance returns to a value closer to the long-term average. Though we do not explicitly account for firn in this model, this effect captures the change in the water budget that would occur as firn/ice above the ELA is exposed.

For example, following the 2003–2004 mass-balance year, which was the most negative in the record and had a greatly reduced AAR (48.6%) compared to the mean 1980–2022 AAR (62.9%) (e.g. Figure 7e), the fractional contribution from ice melt increased by ∼3% while snowmelt decreased by ∼5%. This occurred despite the fact that these two years have similar winter balances (Figure 7a,b), and occurs in other years following the most extreme negative balances (Fig. S10/S11). In fact, in each of the subsequent years following the three most extreme negative mass balances, the relative contribution from glacier-ice melt is maximized (e.g. 66–67% of annual discharge compared to 1980–2022 mean of 61%). Outside of the three most extreme years however, we find that other factors such as the current mass balance complicate the water-budget response.

While we find evidence that the impact of a strongly negative mass balance can carry over into the following year in the most extreme cases, extreme positive mass-balance years do not produce the same effect (Fig. S12–S14). Following extreme positive years, the subsequent water budget still has a reduced fractional contribution from snowmelt and increased contribution from glacier-ice melt, despite having a larger than average accumulation area in the previous year. Relative contributions from glacier-ice melt

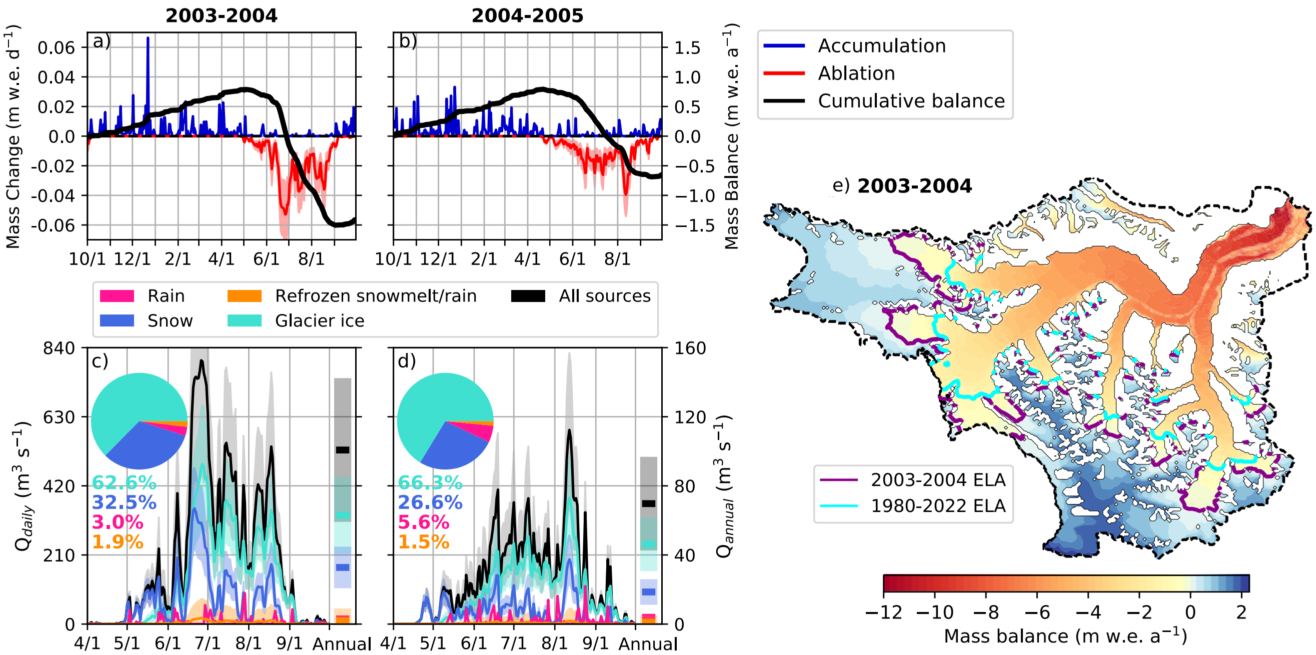

Fig. 7. Mass balance and water budgets corresponding to (a,c) the most negative mass-balance year between 1980–2022 (-1.41 m w.e. a^{-1}), and (b,d) the following year. (e) The distributed mass balance for the 2003–2004 hydrological year (1 Oct–30 Sept), with the 2003–2004 modelled ELA (purple line) compared to the long-term modelled ELA (cyan line). See Fig. S10–S14 for additional examples of water budgets following the most positive and negative mass-balance years.

are indeed minimized (e.g. 53–54% of annual discharge compared to 1980–2022 mean of 61%) during the positive mass-balance years, however, the magnitude of the positive balances estimated for the period 1980–2022 are not high enough to exert an influence on the subsequent year.

4.4.2 Quantifying model sensitivity to climate

Acknowledging that the mass-balance model is structured to have a strong dependence on the temperature and accumulation inputs, we assess the sensitivity of modelled discharge to annual and seasonal air temperatures and accumulation, as well as the annual mass balance to generate hypotheses about how the runoff may change under future climate scenarios. By design in a temperature-index model, melt and thus discharge are both positively correlated with air temperature (Figure 8b,f). However, the enhanced temperature-index melt model is less sensitive to temperature than a classical degree-day model due to the inclusion of potential direct clear sky radiation in the degree-day factor (Hock, 1999). Unsurprisingly, discharge is most strongly correlated with the mean summer (June–August) air temperature (Figure 8c,g). In fact, annual discharge averaged over the five warmest summers between 1980–2022 ($87.20\,\mathrm{m^3\,s^{-1}}$) was approximately double the average during the five coldest summers ($43.76\,\mathrm{m^3\,s^{-1}}$), with little change in the overall water budget (Figure 9a–c). As summer air temperatures rise however, the corresponding increase in annual discharge from glacier-ice melt is double that of snowmelt ($8.38\,\mathrm{m^3\,s^{-1}\,^\circ C^{-1}}$ for glacier-ice melt vs $4.18\,\mathrm{m^3\,s^{-1}\,^\circ C^{-1}}$ for snowmelt) (Figure 8c,g), due to the albedo feedback accounted for in the enhanced temperature-index melt model. Annual discharge from glacier-ice melt and snowmelt are also both, unsurprisingly, inversely correlated with the annual mass balance (Fig. 8a, e). In particular, glacier-ice melt shows a strong inverse correlation with the annual mass balance ($\rho = -0.98$), increasing by an estimated $23.09\,\mathrm{m^3\,s^{-1}}$ for each 1 m w.e. decrease in mass balance. This strong relationship is primarily due to the significant contribution of glacier-ice melt to net ablation (Figure 4b), whereas snowmelt contributes approximately half that of ice melt to net ablation.

Discharge from glacier-ice melt and snowmelt are inversely correlated with summer snowfall ($\rho = -0.52$ and $\rho = -0.78$, respectively; Fig. 8d, h). While high summer snowfall is associated with lower air temperatures, this relationship also captures the importance of summer snowfall on surface albedo (represented in the model by the constraint that the radiation factor for ice must be larger than that for snow). Summers with the least snowfall had, on average, higher annual discharge from glacier-ice melt by $12.68\,\mathrm{m^3\,s^{-1}}$ compared to summers with the greatest snowfall (Figure 9d–f). In contrast, the mass balance

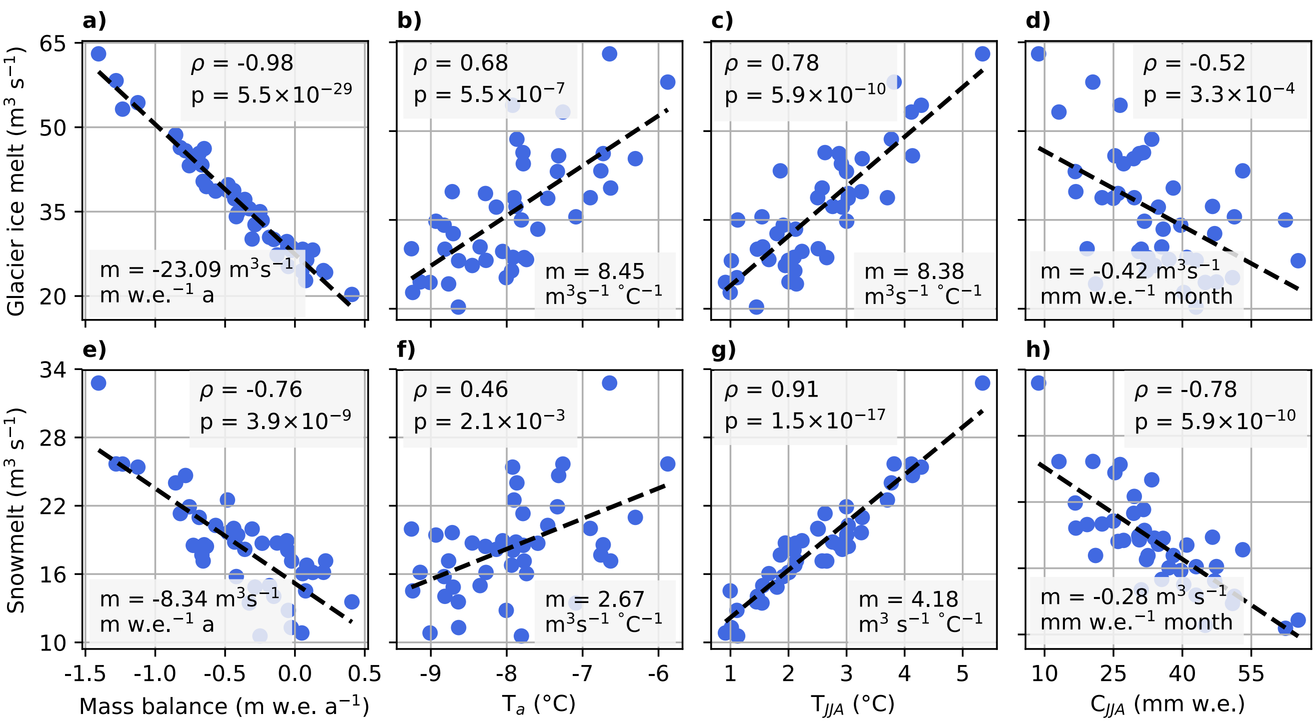

Fig. 8. Relationships between annual discharge from glacier-ice melt (a–d)/snowmelt (e–h) and: (a,e) mass balance, (b,f) mean annual air temperature (T_a), (c,g) mean summer air temperature (T_{JJA}), and (d,h) total summer accumulation (C_{JJA}), fitted with a linear regression. ρ is the Spearman's correlation coefficient, p is the p-value from Spearman's correlation test, and m is the slope of the regression line (dashed).

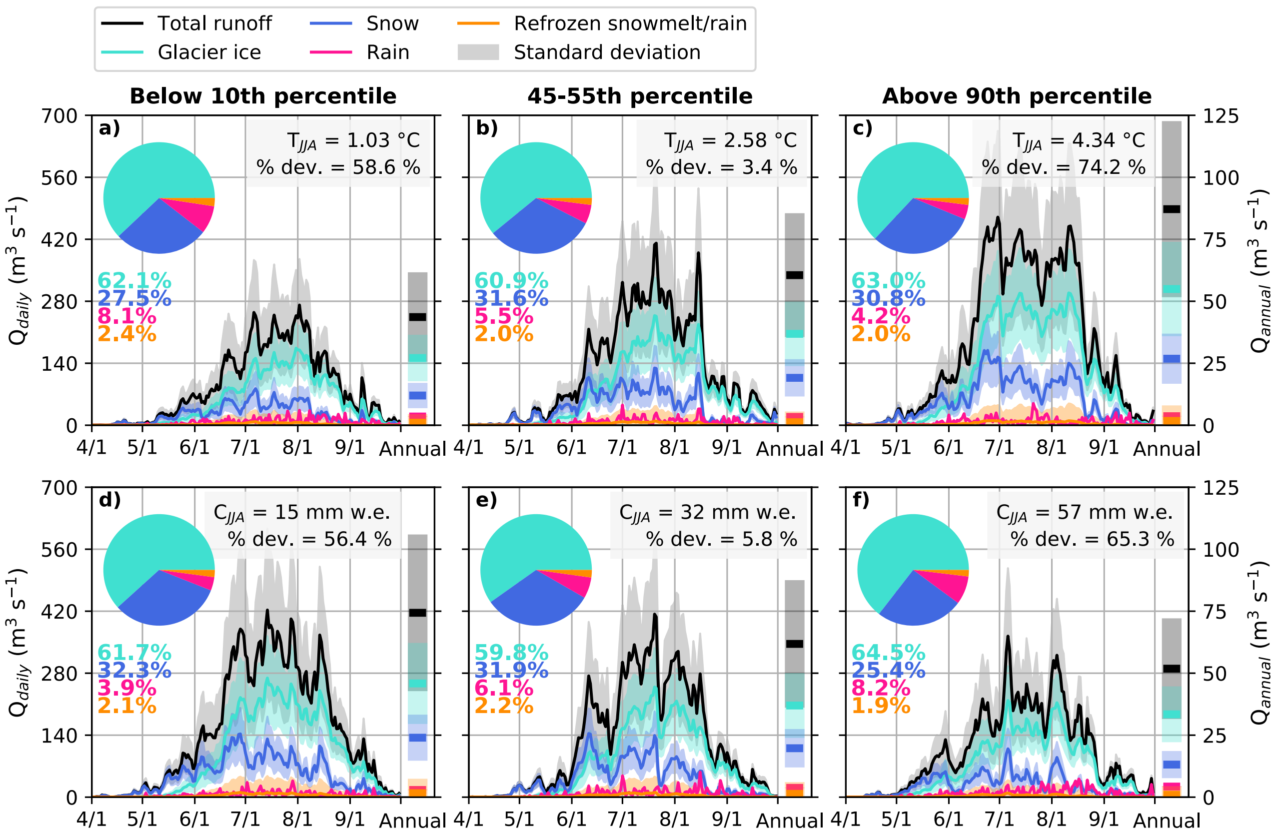

Fig. 9. Hydrographs corresponding to extremes in the summer temperature and accumulation record. Each hydrograph shown is the average of 5 years that fall (a,d) below the 10th percentile, (b,e) between the 45–55th percentile, and (c,f) above the 90th percentile of all years between 1980–2022. Percent deviation refers to deviation from the 1980–2022 mean summer temperature and accumulation.

over the winter season (i.e. the winter balance (Cogley and others, 2010)) is only weakly correlated with glacier-ice melt and has almost no correlation with snowmelt (Fig. S15). This lack of correlation indicates that winter accumulation plays little role in determining the volume of snowmelt during the subsequent ablation season, since the volume of snowmelt is most sensitive to the energy available for melting (i.e. summer air temperatures).

4.5 Expected changes to runoff based on historical sensitivities

Annual discharge from ice and snowmelt are most strongly correlated with summer air temperatures and inversely correlated with summer snowfall (Figure 8), compared to variations in spring, winter, and fall (Fig. S15). As snowmelt and glacier-ice melt are historically the most important components of the water budget in the Kaskawulsh River headwaters (61% and 31% of annual catchment-wide discharge, Figure

4b), we hypothesize that future changes in summer air temperature and summer snowfall will be important drivers of changes in discharge. Rainfall does not exhibit any statistically significant relationships with temperature over the historical period (Fig. S16), so we assume no sensitivity for rainfall in our estimates of future discharge. However, it is likely that rainfall will increase in the future as rising temperatures influence the partitioning of precipitation into rain and snow (Gutiérrez and others, 2021).

Based on CMIP6 projections for SSP5-8.5, summer air temperatures over the Kaskawulsh River headwaters are expected to increase by 1.42°C by 2021–2040, 2.55°C by 2041–2060, and 5.52°C by 2081–2100 relative to 1981–2010 (Figure 10). Assuming the sensitivity of annual glacier-ice melt to summer air temperature is stationary and equal to the historical (1980–2022) value ($8.38\,\mathrm{m^3\,s^{-1}\,{}^\circ C^{-1}}$, Figure 8c), we estimate an increase in glacier-ice melt by a factor of 2.3 by 2081–2100 relative to the 1981–2010 modelled baseline. By 2081–2100, summer snowfall in the catchment is expected to decrease by $0.81\,\mathrm{mm\,w.e.\,day^{-1}}$ ($-25\,\mathrm{mm\,w.e.\,month^{-1}}$ from June–August) according to CMIP6 projections for SSP5-8.5. Again assuming the historical (1980–2022) sensitivity of annual glacier-ice melt to summer snowfall ($-0.42\,\mathrm{m^3\,s^{-1}\,mm\,w.e.^{-1}\,month}$, Figure 8d) is stationary, we estimate a minor increase in glacier-ice melt by a factor of 1.3 relative to the 1981–2010 modelled baseline (Figure 10) due to the decrease in summer snowfall.

While CMIP6 projections indicate decreased snowfall in the catchment during June–August, total June–August precipitation is projected to increase by 19% by 2081–2100 compared to 1981–2010 (Gutiérrez and others, 2021). In addition to increased direct contributions to streamflow from rainfall, snowmelt also generally increases during rain-on-snow events (e.g. Marks and others, 2001; Kormos and others, 2014), which may become more common in the future as rising air temperatures allow liquid precipitation to occur at higher elevations. The predicted sensitivities to future temperature and snowfall, assessed separately, likely underestimate the true change in future runoff since the combined effects of changes in both summer temperature and summer snowfall may enhance the response of runoff beyond the sum of their individual influences.

In these estimates of future runoff we assume no change in area of the Kaskawulsh Glacier, however future reductions in glacier area will inevitably influence runoff. Projections of the Kaskawulsh Glacier from a global glacier-modelling study (Rounce and others, 2023) suggest that this assumption should have minimal impact on our results within the remainder of the century: while a ∼46% reduction in glacier mass is projected by 2100 relative to 2001–2020 under SSP5-8.5, this is accompanied by only a 7.5% reduction in glacier area, equivalent to $\sim$79 km^2. The same projections indicate that runoff from the Kaskawulsh Glacier will likely continue to increase through the remainder of the century, with peak water not expected to occur until after 2100.

5 DISCUSSION

5.1 Regional glacier mass loss

Several other studies have estimated mass loss in the region through a variety of methods, both individually for the Kaskawulsh Glacier (e.g. Larsen and others, 2015; Berthier and others, 2010; Foy and others, 2011) and at the regional scale (e.g. Hugonnet and others, 2021) for periods bracketed by our study period. The mass loss of Kaskawulsh Glacier that we estimate from 1995–2013 (-0.38 ± 0.16 m w.e. a^{-1}) agrees within uncertainty with that estimated by Larsen and others (2015) for the same period using repeat laser altimetry (-0.35 m w.e. a^{-1}). Our 1979–2007 estimate (-0.33 ± 0.15 m w.e. a^{-1}) is also in agreement within uncertainty with the 1977–2007 geodetic estimate from Berthier and others (2010) (-0.46 ± 0.20 m w.e. a^{-1}).

The St. Elias Mountains alone represent about 38% of the total glacierized area of 33,174 km^2 in the Yukon–Alaska region (Randolph Glacier Inventory, version 6.0) (Arendt and others, 2017) and have experienced an estimated mass change rate of -23.3 Gt a^{-1} from 2000–2019 (Hugonnet and others, 2021) (35% of the Yukon–Alaska regional mass loss). The Kaskawulsh River Headwaters represent 3.5% of the glacier area in the St. Elias Mountains, but just 2.2% of the estimated 2000–2019 mass loss, based on our model results (-0.52 ± 0.17 Gt a^{-1}). This finding is not unexpected, given the geographic location of the catchment on the continental side of the range, where glaciers are under-contributing to regional mass loss relative to their maritime counterparts (e.g. Jakob and others, 2020; Jin and others, 2017).

5.2 Comparison with hydrological regimes in other glacierized catchments

Glacier ice-melt contributions to total runoff vary across glacierized catchments based on climate, basin hypsometry, and glacier mass balance (e.g. Huss, 2011). In many cases, the fractional contribution of glacier-ice melt to catchment-wide runoff is also related to the fraction of glacierized area in the catchment (e.g. Farinotti and others, 2012). In the Kaskawulsh River Headwaters (69% glacierized), we estimate that glacier-ice melt accounts for an average of 61% of the annual catchment-wide discharge from 1980–2022 (Figure 4b). The Gulf of Alaska watershed, to which the Alsek River basin is a major contributor, has 17% glacier-covered area, with glacier-ice melt accounting for 17% of the annual discharge between 1980–2014

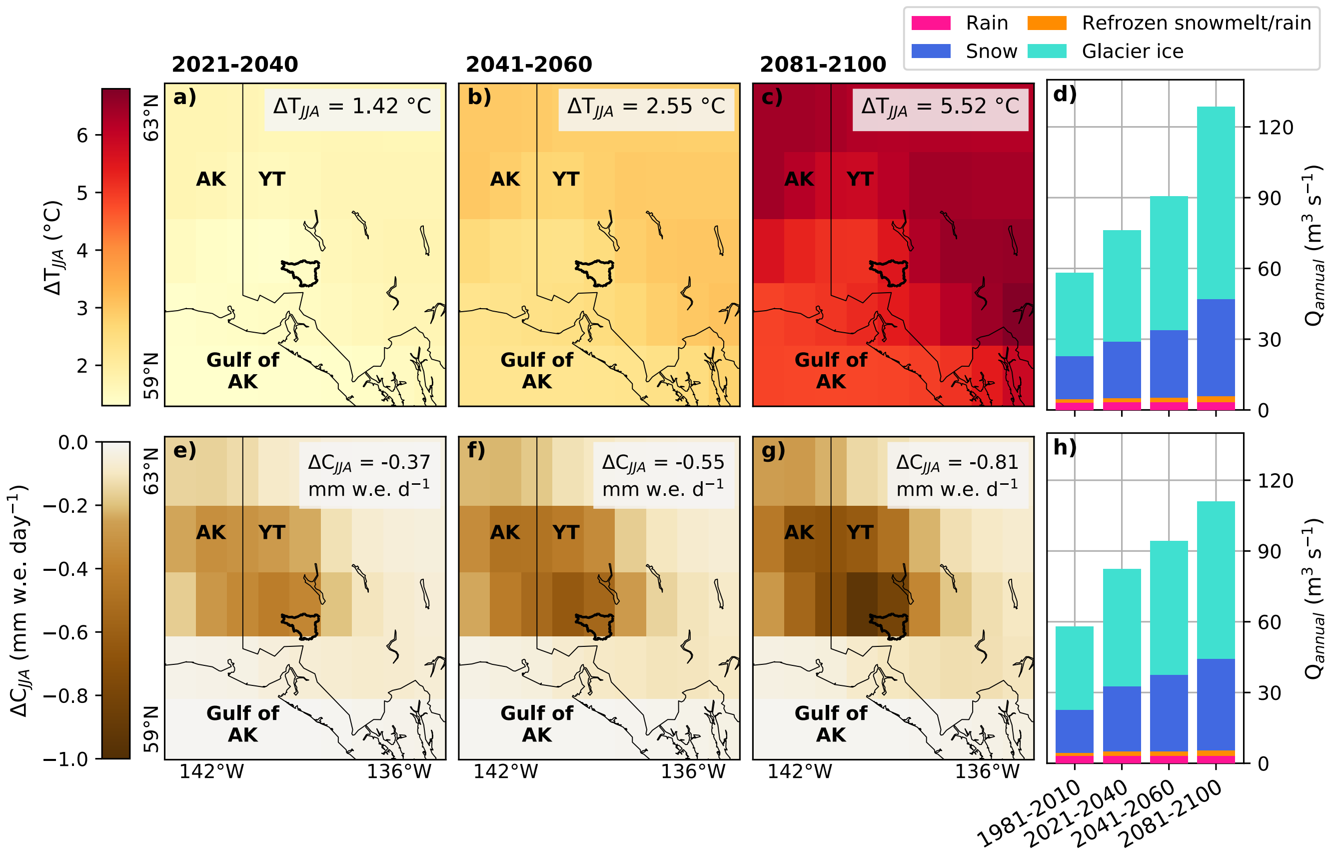

Fig. 10. Projections of future summer air-temperature change (ΔT_{JJA}) (a–c) and summer snowfall (ΔC_{JJA}) (e–f) from CMIP6 for SSP5-8.5 (Gutiérrez and others, 2021), with values from the gridcell with the greatest overlap with the Kaskawulsh River headwaters (thick black outline) printed in the top right corner of each panel. (d,h): Historical discharge (1981–2010) estimated in this study, and future discharge assessed individually for changes in summer air temperature (d) and summer snowfall (h). Future estimates are computed by multiplying the historical sensitivities (Figure 8) by the projected changes for the three future time periods and adding the result to modelled 1981–2010 discharge.

(Beamer and others, 2016). In the rainfall-dominated Kumalak River Basin (21% glacierized) in High Mountain Asia, glacier-ice melt contributes 28% of the total runoff, while snowmelt contributes 11% and rainfall the remaining 61% (Li and others, 2020). Across nine high-alpine catchments in the Swiss Alps with 7–63% glacierized areas, maximum glacier ice-melt contributions estimated for 1900–2100 using a glacier evolution and runoff model range from 6–49% depending on the glacierized fraction (Farinotti and others, 2012), and in the 59% glacierized Blatten catchment in the Swiss Alps, contributions from glacier-ice melt contributed 47–55% of the annual discharge between 1988–2008 (Huss, 2011).

The relative contributions of glacier-ice melt to annual discharge in the Kaskawulsh River headwaters fluctuate minimally on an interannual basis (53–67% from 1980–2022) (Figure 4). In other climate regimes, such as the semi-arid Chilean Andes, there is evidence of much larger fluctuations in the water budget in response to extreme weather events, particularly where glacier-ice melt constitutes an important contribution to streamflow during the dry season in late summer to early fall (e.g. Burger and others, 2019; Bravo and others, 2017). At Rio del Yeso basin in central Chile (18% glacierized), annual contributions from glacier melt ranged between 3–32% from 2000–2015 depending on the severity of the dry season (Burger and others, 2019). In the Kaskawulsh River headwaters however, interannual discharge variability from glacier-ice melt decreased over 1980–2022, a natural consequence of the progression towards peak water and a trend that signifies the increasing influence of ice melt on the water budget. As the glacier retreats and ultimately passes peak water in the future, we can expect discharge variability to increase as the glacier exerts a progressively weaker influence on catchment-wide discharge (e.g. Baraër and others, 2012), making the discharge from the catchment more sensitive to interannual climate variability.

5.3 Future outlook and downstream impacts

In the short term, increasing discharge in the Kaskawulsh River headwaters may increase downstream sediment transport and erosion (Milner and others, 2017), and elevate the potential for geohazards such as high peak annual discharge and floods (e.g. Ragettli and others, 2016). Based on the strong historical correlation between summer air temperature and ice and snowmelt (Figure 8c,g), we also anticipate that changes in summer air temperature will likely have a large impact on future discharge in this region (Figure 10). High correlations between summer air temperatures and ice melt have been reported for other continental glaciers in western North America (e.g. O'Neel and others, 2014; Fleming and Clarke, 2003; Moore and Demuth, 2001), in contrast to coastal glaciers, which are typically influenced by large seasonal snowpacks and significant summer rainfall which contribute more consistently to discharge (e.g. O'Neel and others, 2014).

Discharge from the Kaskawulsh River headwaters is also strongly inversely correlated with the annual glacier mass balance (Figure 8a,e), however this correlation is predominantly related to the correlation between discharge and ablation. In some cases, an extremely negative balance can result in excess ice melt in the following year due to a depletion of the multi-year snowpack above the equilibrium line (Figure 7). On the Columbia Glacier in Washington, USA, three consecutive years of significant negative annual balances from 2003–2005 led to a similar mode of mass loss with a more extreme outcome: the complete loss of the accumulation zone and significant thinning at high elevations following the period of strong negative balances (Pelto, 2011). In contrast with the effect of extreme negative balance years, we find no examples of positive mass balances in our modelled record high enough to inhibit ice melt during the following ablation season, unlike for the maritime Wolverine Glacier in Alaska where winter accumulation has been known to reduce mass loss during the following ablation season (O'Neel and others, 2014). We therefore expect that future mass changes of the Kaskawulsh Glacier will be primarily driven by temperature rather than precipitation.

Although changes in glacier area are not incorporated in the mass-balance model, projections suggest that the Kaskawulsh Glacier will experience limited retreat relative to its current size during the remainder of the century, with an estimated area loss of 7.5% by 2100 relative to 2001–2020 under SSP5-8.5 (Rounce and others, 2023). This is consistent with the glacier's substantial ice thickness in the terminus region ($\sim$400–600 m) (Main and others, 2023), the presence of widespread insulating debris cover (Robinson and others, in review), and the glacier's historically slow response to mass imbalance (e.g. Young and others, 2021; Foy and others, 2011). In northwest British Columbia and southwest Yukon, the dominant mode of glacier mass loss in response to an increase in temperature thus far has been thinning without significant terminus retreat (e.g. Moore and others, 2009). Until sustained thinning of the terminus region of the Kaskawulsh Glacier (e.g. Main and others, 2023) leads to significant retreat, it will amplify meltwater production due to surface-elevation feedbacks.

6 CONCLUSION

This study employs a mass-balance model driven by downscaled and bias-corrected climate reanalysis data to estimate the glacier mass loss, discharge, and water budget of the Kaskawulsh River headwaters over four decades from 1980–2022. We conduct statistical analyses on timeseries of modelled temperature, precipitation, and discharge to quantify temporal trends, and identify correlations between climatic and discharge variables with which we estimate the sensitivity of modelled runoff to climate change.

Glaciers in the Kaskawulsh River headwaters are estimated to have lost 18.02 Gt of mass between 1980–2022 ($-0.38\,\mathrm{m\,w.e.\,a^{-1}}$), accounting for 2.2% of the estimated mass loss in the St. Elias Mountains as a whole between 2000–2019, an under-contribution given that these glaciers represent 3.5% of the total glacierized area in the St. Elias Mountains. Since the 1980s the average annual mass-loss rate has increased with each subsequent decade, more than doubling from $-0.22 \pm 0.13\,\mathrm{m\,w.e.\,a^{-1}}$ from 1980–1989 to $-0.49 \pm 0.17\,\mathrm{m\,w.e.\,a^{-1}}$ from 2010–2019. This trend is accompanied by an earlier onset of net ablation in the catchment by $\sim$5 days per decade. The rerouting of meltwater from the Ä'äy Chù to the Kaskawulsh River in 2016 produced a substantial increase in discharge in the Alsek River, with discharge from the Kaskawulsh River Headwaters accounting for an estimated 22–29% of the annual discharge measured at the downstream hydrometric station on the Alsek River above Bates River after 2016. This rerouting also resulted in an estimated 5–11% increase in water delivery from the Alsek River to the Gulf of Alaska.

Mean ablation season (May–August) discharge from glacier-ice melt increased at a statistically-significant rate of $7.7\,\mathrm{m^3\,s^{-1}}$ per decade, while peak annual discharge from glacier-ice melt occurred 3.5 days earlier per decade. Meanwhile, the annual variability of glacier-ice melt discharge (and total discharge) decreased. These trends are evidence that the Kaskawulsh River headwaters is in the early stages of progressing toward "peak water" (Baraër and others, 2012). Mean ablation-season discharge from rain also increased at a statistically significant rate of $1.0\,\mathrm{m^3\,s^{-1}}$ per decade, an indication that rainfall may become an increasingly important component of the water budget in the future, especially in August and September.

The annual water budget varies depending on temperature and precipitation, with glacier-ice melt accounting for 53–67% (mean of 61%) of annual catchment-wide discharge, snowmelt accounting for 20–38% (mean of 31%), rain accounting for 2–11% (mean of 6%), and melt from refrozen snowmelt/rain accounting for 1–3% (mean of 2%). We find that maximum contributions from glacier-ice melt (66–67%) to annual discharge typically occur in the year following an extreme negative mass-balance year. This result suggests that a significant increase in the equilibrium line altitude can precondition the glacier surface for enhanced ice melt the following summer. High rates of summer snowfall may serve to dampen ice melt by temporarily increasing the surface albedo, however, summer snowfall rates are projected to decrease in the future along with a concurrent increase in summer temperatures. We hypothesize a more than doubling (2.3×) of annual runoff by 2080–2100 based summer air-temperature increases projected by CMIP6 (SSP5-8.5) and the sensitivity of modelled runoff to summer air temperature calculated over the historical period of 1980–2022.

Other large glaciers in the region will likely undergo comparable hydrological changes driven by ongoing climate change, while smaller glaciers may already be experiencing a post-peak-water decline in runoff. The resulting shifts in the hydrological system are expected to affect streamflow and temperature, alter sediment and nutrient delivery to aquatic ecosystems (e.g. Hood and Berner, 2009), and impact habitat conditions for key species such as salmon (e.g. Moore and others, 2023; Pitman and others, 2021). Coupled mass-balance and ice-dynamics model projections are needed to simulate the competing effects of glacier area loss and enhanced melt under future warming scenarios. A broader investigation of this nature will help provide a more comprehensive picture of the regional hydrological response to climate change, from which we can begin to anticipate the downstream ecological, environmental, and socioeconomic impacts.

7 SUPPLEMENTARY MATERIAL

Supplementary material for this article can be found at [doi].

8 DATA AVAILABILITY

Daily and annual discharge data from the Dezadeash River, Alsek River above Bates River, and Alsek River near Yakutat hydrometric stations were downloaded from the Environment and Climate Change Canada Historical Hydrometric Data web site `https://wateroffice.ec.gc.ca/mainmenu/historical_data_index_e.html`. The Kaskawulsh Glacier outline was obtained from `https://www.glims.org/maps/glims`. The raw NARR data downscaled for this study were obtained from `https://downloads.psl.noaa.gov/Datasets/NARR`, and the downscaled temperature data for the Kaskawulsh River Headwaters can be found at: `https://doi.org/10.5281/zenodo.14010407`, and downscaled precipitation data can be found at: `https://doi.org/10.5281/zenodo.14014495`. Other inputs used to run the mass-balance model can be downloaded at: `https://doi.org/10.5281/zenodo.14010158`. The model outputs (spanning 1980–2022) used to conduct the analyses presented in this paper can be downloaded at: `https://doi.org/10.5281/zenodo.14010257`. Downscaling and melt-model code will be made public on github upon manuscript publication.

9 ACKNOWLEDGEMENTS

The Kaskawulsh River headwaters study site is located within the Traditional Territories of the Kluane, Champagne & Aishihik, and White River First Nations. We thank E. Berthier for providing the DEMs used in downscaling and helping with the interpretation, E. Young for providing the original downscaling and melt-model code and for helping with many aspects of using the model, and B. Tober for providing the future projections of glacier area change for the Kaskawulsh Glacier. KR and GF are grateful for financial support provided by the Natural Sciences and Engineering Research Council of Canada, Simon Fraser University, and Environment and Climate Change Canada. MB was supported by Natural Sciences and Engineering Research Council of Canada under grant Nos. RGPIN-2020-05612 and RGPNS-2020-05612. DR was supported by NASA under grant Nos. 80NSSC20K1296 and 80NSSC20K1595.

10 AUTHOR CONTRIBUTIONS

GF conceived of the original study and KR/GF co-developed the details. KR developed the model code, tuned and ran the mass-balance model, and performed the analysis of model output. KR led the manuscript preparation, with contributions from GF, MB, and DR. All authors contributed to various aspects of the interpretation and edited the manuscript.

REFERENCES

Arendt A, Bliss A, Bolch T, Cogley J, Gardner A, Hagen JO, Hock R, Huss M, Kaser G, Kienholz C and others (2017) Randolph Glacier Inventory–a dataset of global glacier outlines: Version 6.0: Technical report, global land ice measurements from space

Azam MF and Srivastava S (2020) Mass balance and runoff modelling of partially debris-covered Dokriani Glacier in monsoon-dominated Himalaya using ERA5 data since 1979. *Journal of Hydrology*, **590**, 125432

Bachelder J, Cadieux M, Liu-Kang C, Lambert P, Filoche A, Galhardi JA, Hadioui M, Chaput A, Bastien-Thibault MP, Wilkinson KJ and others (2020) Chemical and microphysical properties of wind-blown dust near an actively retreating glacier in Yukon, Canada. *Aerosol Science and Technology*, **54**(1), 2–20

Baraër M, Mark BG, McKenzie JM, Condom T, Bury J, Huh KI, Portocarrero C, Gómez J and Rathay S (2012) Glacier recession and water resources in Peru's Cordillera Blanca. *Journal of Glaciology*, **58**(207), 134–150

Beamer J, Hill D, Arendt A and Liston G (2016) High-resolution modeling of coastal freshwater discharge and glacier mass balance in the Gulf of Alaska watershed. *Water Resources Research*, **52**(5), 3888–3909

Berthier E, Schiefer E, Clarke GKC, Menounos B and Rémy F (2010) Contribution of Alaskan glaciers to sea-level rise derived from satellite imagery. *Nature Geoscience*, **3**(2), 92–95 (doi: 10.1038/ngeo737)

Bliss A, Hock R and Radić V (2014) Global response of glacier runoff to twenty-first century climate change. *Journal of Geophysical Research: Earth Surface*, **119**(4), 717–730 (doi: 10.1002/2013JF002931)

Brabets TP and Walvoord MA (2009) Trends in streamflow in the Yukon River Basin from 1944 to 2005 and the influence of the Pacific Decadal Oscillation. *Journal of Hydrology*, **371**(1-4), 108–119

Bravo C, Loriaux T, Rivera A and Brock BW (2017) Assessing glacier melt contribution to streamflow at Universidad Glacier, central Andes of Chile. *Hydrology and Earth System Sciences*, **21**(7), 3249–3266

Burger F, Ayala A, Farias D, Shaw TE, MacDonell S, Brock B, McPhee J and Pellicciotti F (2019) Interannual variability in glacier contribution to runoff from a high-elevation Andean catchment: understanding the role of debris cover in glacier hydrology. *Hydrological Processes*, **33**(2), 214–229

Chesnokova A, Baraër M, Laperrière-Robillard T and Huh K (2020) Linking mountain glacier retreat and hydrological changes in southwestern Yukon. *Water Resources Research*, **56**(1), e2019WR025706 (doi: 10.1029/2019WR025706)

Clarke GKC and Holdsworth G (2002) Glaciers of the St. Elias Mountains. *US Geological Survey professional paper*

Cogley JG, Arendt A, Bauder A, Braithwaite R, Hock R, Jansson P, Kaser G, Moller M, Nicholson L, Rasmussen L and others (2010) Glossary of glacier mass balance and related terms. *IHP-VII Technical Documents in Hydrology No. 86, IACS Contribution No. 2, UNESCO-IHP, Paris.*

Farinotti D, Usselmann S, Huss M, Bauder A and Funk M (2012) Runoff evolution in the Swiss Alps: Projections for selected high-alpine catchments based on ensembles scenarios. *Hydrological Processes*, **26**(13), 1909–1924 (doi: 10.1002/hyp.8276)

Farinotti D, Huss M, Fürst JJ, Landmann J, Machguth H, Maussion F and Pandit A (2019) A consensus estimate for the ice thickness distribution of all glaciers on Earth. *Nature Geoscience*, **12**(3), 168–173 (doi: 10.1038/s41561-019-0300-3)

Fleming SW and Clarke GKC (2003) Glacial control of water resource and related environmental responses to climatic warming: empirical analysis using historical streamflow data from northwestern Canada. *Canadian Water Resources Journal*, **28**(1), 69–86

Foy N, Copland L, Zdanowicz C, Demuth M and Hopkinson C (2011) Recent volume and area changes of Kaskawulsh Glacier, Yukon, Canada. *Journal of Glaciology*, **57**(203), 515–525 (doi: 10.3189/002214311796905596)

Gidden MJ, Riahi K, Smith SJ, Fujimori S, Luderer G, Kriegler E, Van Vuuren DP, Van Den Berg M, Feng L, Klein D and others (2019) Global emissions pathways under different socioeconomic scenarios for use in CMIP6: a dataset of harmonized emissions trajectories through the end of the century. *Geoscientific model development*, **12**(4), 1443–1475

Goss GA (2021) *Glacier retreat and fluvial landscape response*. Ph.D. thesis, University of Calgary

Guan H, Wilson JL and Xie H (2009) A cluster-optimizing regression-based approach for precipitation spatial downscaling in mountainous terrain. *Journal of Hydrology*, **375**(3-4), 578–588 (doi: 10.1016/j.jhydrol.2009.07.007)

Gutiérrez J, Jones R, Narisma G, Alves L, Amjad M, Gorodetskaya I, Grose M, Klutse N, Krakovska S, Li J, Martínez-Castro D, Mearns L, Mernild S, Ngo-Duc T, van den Hurk B and Yoon JH (2021) *Atlas. In Climate Change 2021: The Physical Science Basis. Contribution of Working Group I to the Sixth Assessment Report of the Intergovernmental Panel on Climate Change*. Cambridge University Press, Cambridge, UK and New York, NY, USA (doi: 10.1017/9781009157896)

Hamed KH and Rao AR (1998) A modified Mann-Kendall trend test for autocorrelated data. *Journal of hydrology*, **204**(1-4), 182–196

Hock R (1999) A distributed temperature-index ice-and snowmelt model including potential direct solar radiation. *Journal of Glaciology*, **45**(149), 101–111 (doi: 10.3189/S0022143000003087)

Hock R (2003) Temperature index melt modelling in mountain areas. *Journal of Hydrology*, **282**(1-4), 104–115 (doi: 10.1016/S0022-1694(03)00257-9)

Hood E and Berner L (2009) Effects of changing glacial coverage on the physical and biogeochemical properties of coastal streams in southeastern Alaska. *Journal of Geophysical Research: Biogeosciences*, **114**(G3)

Huck R, Bryant RG and King J (2023) The (mis) identification of high-latitude dust events using remote sensing methods in the Yukon, Canada: a sub-daily variability analysis. *Atmospheric Chemistry and Physics*, **23**(11), 6299–6318

Hugonnet R, McNabb R, Berthier E, Menounos B, Nuth C, Girod L, Farinotti D, Huss M, Dussaillant I, Brun F and others (2021) Accelerated global glacier mass loss in the early twenty-first century. *Nature*, **592**(7856), 726–731 (doi: 10.1038/s41586-021-03436-z)

Huss M (2011) Present and future contribution of glacier storage change to runoff from macroscale drainage basins in Europe. *Water Resources Research*, **47**(7) (doi: 10.1029/2010WR010299)

Huss M and Hock R (2018) Global-scale hydrological response to future glacier mass loss. *Nature Climate Change*, **8**(2), 135–140 (doi: 10.1038/s41558-017-0049-x)

Huybrechts P and De Wolde J (1999) The dynamic response of the Greenland and Antarctic ice sheets to multiple-century climatic warming. *Journal of Climate*, **12**(8), 2169–2188

IPCC (2021) *Climate Change 2021: The Physical Science Basis. Contribution of Working Group I to the Sixth Assessment Report of the Intergovernmental Panel on Climate Change*. Cambridge University Press, Cambridge, UK and New York, NY, USA (doi: 10.1017/9781009157896)

Jakob L, Gourmelen N, Ewart M and Plummer S (2020) Ice loss in High Mountain Asia and the Gulf of Alaska observed by CryoSat-2 swath altimetry between 2010 and 2019

Janssens I and Huybrechts P (2000) The treatment of meltwater retention in mass-balance parameterizations of the Greenland ice sheet. *Annals of Glaciology*, **31**, 133–140 (doi: 10.3189/172756400781819941)

Jarosch AH, Anslow FS and Clarke GKC (2012) High-resolution precipitation and temperature downscaling for glacier models. *Climate Dynamics*, **38**, 391–409 (doi: 10.1007/s00382-010-0949-1)

Jin S, Zhang T and Zou F (2017) Glacial density and GIA in Alaska estimated from ICESat, GPS and GRACE measurements. *Journal of Geophysical Research: Earth Surface*, **122**(1), 76–90

Kendall MG (1948) Rank correlation methods.

Kormos PR, Marks D, McNamara JP, Marshall H, Winstral A and Flores AN (2014) Snow distribution, melt and surface water inputs to the soil in the mountain rain–snow transition zone. *Journal of Hydrology*, **519**, 190–204

La Frenierre J and Mark BG (2014) A review of methods for estimating the contribution of glacial meltwater to total watershed discharge. *Progress in Physical Geography*, **38**(2), 173–200 (doi: 10.1177/0309133313516161)

Larsen C, Burgess E, Arendt A, O'neel S, Johnson A and Kienholz C (2015) Surface melt dominates Alaska glacier mass balance. *Geophysical Research Letters*, **42**(14), 5902–5908

Li J, Rodriguez-Morales F, Fettweis X, Ibikunle O, Leuschen C, Paden J, Gomez-Garcia D and Arnold E (2023) Snow stratigraphy observations from Operation IceBridge surveys in Alaska using S and C band airborne ultra-wideband FMCW (frequency-modulated continuous wave) radar. *The Cryosphere*, **17**(1), 175–193 (doi: 10.5194/tc-17-175-2023)

Li Z, Shi X, Tang Q, Zhang Y, Gao H, Pan X, Déry SJ and Zhou P (2020) Partitioning the contributions of glacier melt and precipitation to the 1971–2010 runoff increases in a headwater basin of the Tarim River. *Journal of Hydrology*, **583**, 124579 (doi: 10.1016/j.jhydrol.2020.124579)

Main B, Copland L, Smeda B, Kochtitzky W, Samsonov S, Dudley J, Skidmore M, Dow C, Van Wychen W, Medrzycka D and others (2023) Terminus change of Kaskawulsh Glacier, Yukon, under a warming climate: retreat, thinning, slowdown and modified proglacial lake geometry. *Journal of Glaciology*, **69**(276), 936–952 (doi: 10.1017/jog.2022.114)

Mann HB (1945) Nonparametric tests against trend. *Econometrica: Journal of the econometric society*, 245–259

Mantua NJ and Hare SR (2002) The Pacific decadal oscillation. *Journal of oceanography*, **58**, 35–44

Marks D, Link T, Winstral A and Garen D (2001) Simulating snowmelt processes during rain-on-snow over a semi-arid mountain basin. *Annals of Glaciology*, **32**, 195–202

Mesinger F, DiMego G, Kalnay E, Mitchell K, Shafran PC, Ebisuzaki W, Jović D, Woollen J, Rogers E, Berbery EH and others (2006) North American regional reanalysis. *Bulletin of the American Meteorological Society*, **87**(3), 343–360 (doi: 10.1175/BAMS-87-3-343)

Milner AM, Khamis K, Battin TJ, Brittain JE, Barrand NE, Füreder L, Cauvy-Fraunié S, Gíslason GM, Jacobsen D, Hannah DM and others (2017) Glacier shrinkage driving global changes in downstream systems. *Proceedings of the National Academy of Sciences*, **114**(37), 9770–9778

Moore JW, Pitman KJ, Whited D, Marsden NT, Sexton EK, Sergeant CJ and Connor M (2023) Mining stakes claim on salmon futures as glaciers retreat. *Science*, **382**(6673), 887–889

Moore R and Demuth M (2001) Mass balance and streamflow variability at Place Glacier, Canada, in relation to recent climate fluctuations. *Hydrological Processes*, **15**(18), 3473–3486

Moore R, Fleming S, Menounos B, Wheate R, Fountain A, Stahl K, Holm K and Jakob M (2009) Glacier change in western North America: influences on hydrology, geomorphic hazards and water quality. *Hydrological Processes: An International Journal*, **23**(1), 42–61

Naegeli K and Huss M (2017) Sensitivity of mountain glacier mass balance to changes in bare-ice albedo. *Annals of Glaciology*, **58**(75pt2), 119–129

Neal EG, Hood E and Smikrud K (2010) Contribution of glacier runoff to freshwater discharge into the Gulf of Alaska. *Geophysical Research Letters*, **37**(6), L06404 (doi: 10.1029/2010GL042385)

Østrem G (1959) Ice melting under a thin layer of moraine, and the existence of ice cores in moraine ridges. *Geografiska Annaler*, **41**(4), 228–230 (doi: 10.1080/20014422.1959.11907953)

O'Neel S, Hood E, Arendt A and Sass L (2014) Assessing streamflow sensitivity to variations in glacier mass balance. *Climatic Change*, **123**, 329–341

Pelto M (2011) Skykomish River, Washington: Impact of ongoing glacier retreat on streamflow. *Hydrological Processes*, **25**(21), 3356–3363

Pitman KJ, Moore JW, Huss M, Sloat MR, Whited DC, Beechie TJ, Brenner R, Hood EW, Milner AM, Pess GR and others (2021) Glacier retreat creating new Pacific salmon habitat in western North America. *Nature Communications*, **12**(1), 6816 (doi: 10.1038/s41467-021-26897-2)

Ragettli S, Immerzeel WW and Pellicciotti F (2016) Contrasting climate change impact on river flows from high-altitude catchments in the Himalayan and Andes Mountains. *Proceedings of the National Academy of Sciences*, **113**(33), 9222–9227

RGI Consortium (2017) Randolph Glacier Inventory–a dataset of global glacier outlines: Version 6.0: Technical report, global land ice measurements from space (doi: 10.7265/N5-RGI-60)

Robinson K (2024) *Reconstructing a multi-decadal runoff record for a highly-glacierized catchment in Yukon, Canada.* Master's thesis, Simon Fraser University

Robinson KM, Flowers GE and Rounce DR (in review) Sensitivity of modelled mass balance and runoff to representations of debris and accumulation on the Kaskawulsh Glacier, Yukon, Canada. [preprint] (doi: https://doi.org/10.31223/X5FX3W)

Rounce DR, Hock R, McNabb R, Millan R, Sommer C, Braun M, Malz P, Maussion F, Mouginot J, Seehaus T and others (2021) Distributed global debris thickness estimates reveal debris significantly impacts glacier mass balance. *Geophysical Research Letters*, **48**(8), GL091311 (doi: 10.1029/2020GL091311)

Rounce DR, Hock R, Maussion F, Hugonnet R, Kochtitzky W, Huss M, Berthier E, Brinkerhoff D, Compagno L, Copland L and others (2023) Global glacier change in the 21st century: Every increase in temperature matters. *Science*, **379**(6627), 78–83 (doi: 10.1126/science.abo1324)

Sen PK (1968) Estimates of the regression coefficient based on Kendall's tau. *Journal of the American statistical association*, **63**(324), 1379–1389

Shugar DH, Clague JJ, Best JL, Schoof C, Willis MJ, Copland L and Roe GH (2017) River piracy and drainage basin reorganization led by climate-driven glacier retreat. *Nature Geoscience*, **10**(5), 370–375 (doi: 10.1038/ngeo2932)

Spearman C (1904) The proof and measurement of association between two things. *American Journal of Psychology*, **15**, 88

Warren SG (2019) Optical properties of ice and snow. *Philosophical Transactions of the Royal Society A*, **377**(2146), 20180161 (doi: 10.1098/rsta.2018.0161)

Wheler BA and Flowers GE (2011) Glacier subsurface heat-flux characterizations for energy-balance modelling in the Donjek Range, southwest Yukon, Canada. *Journal of Glaciology*, **57**(201), 121–133

Young EM, Flowers GE, Berthier E and Latto R (2021) An imbalancing act: the delayed dynamic response of the Kaskawulsh Glacier to sustained mass loss. *Journal of Glaciology*, **67**(262), 313–330 (doi: 10.1017/jog.2020.107)

Young JC, Arendt A, Hock R and Pettit E (2018) The challenge of monitoring glaciers with extreme altitudinal range: mass-balance reconstruction for Kahiltna Glacier, Alaska. *Journal of Glaciology*, **64**(243), 75–88 (doi: 10.1017/jog.2017.80)

Zemp M, Huss M, Thibert E, Eckert N, McNabb R, Huber J, Barandun M, Machguth H, Nussbaumer SU, Gärtner-Roer I and others (2019) Global glacier mass changes and their contributions to sea-level rise from 1961 to 2016. *Nature*, **568**(7752), 382–386 (doi: 10.1038/s41586-019-1071-0)